Center for Nuclear Waste Regulatory Analyses

6220 CULEBRA ROAD • P.O. DRAWER 28510 • SAN ANTONIO, TEXAS, U.S.A. 78228-0510
(210) 522-5160 • FAX (210) 522-5184

July 3, 1996
Contract No. NRC-02-93-005
Account No. 20-5708-861

U.S. Nuclear Regulatory Commission
Attn: Mr. Neil Coleman
Technical Leader
Engineering and Geosciences Branch
Mail Stop 7 D13
Washington, DC 20555

Subject: Completion of Intermediate Milestone: "Simulating the Spatial Distribution of Infiltration at Yucca Mountain, Nevada" (IM 20-5708-861-680)

Dear Mr. Coleman:

The subject paper is specified as Intermediate Milestone 20-5708-861-680 in the CNWRA Operations Plans for the Key Technical Issue (KTI) Unsaturated and Saturated Flow Under Isothermal Conditions, as modified by Table 2 of the CNWRA Program Manager's Periodic Report for Period 5 - FY96. After programmatic acceptance by the NRC, this paper will be submitted for publication in *Water Resources Research*.

This deliverable is submitted for your review and acceptance. If you have any questions regarding this deliverable, please call me at (210) 522-5540 or Dr. Stuart Stothoff at (210) 522-5208.

Sincerely,

English C. Pearcy
Element Manager
Geohydrology & Geochemistry

cc: J. Linehan
S. Fortuna
B. Stiltenpole
B. Meehan
J. Greeves
M. Federline
J. Austin
D. Brooks
F. Ross
M. Bell
J. Thoma
B. Leslie
T. Nicholson
W. Patrick
CNWRA Directors
CNWRA Element Managers
G. Wittmeyer
R. Bagtzoglou
S. Stothoff
R. Green
S. Rowe (SwRI)
W. Ford

Washington Office • Twinbrook Metro Plaza, #210 • 12300 Twinbrook Parkway • Rockville, Maryland 20852-1606

SIMULATING THE SPATIAL DISTRIBUTION OF INFILTRATION AT YUCCA MOUNTAIN, NEVADA

Stuart A. Stothoff, Hannah M. Castellaw, and Amvrossios C. Bagtzoglou
Center for Nuclear Waste Regulatory Analyses
6220 Culebra Road
San Antonio, TX 78238-5166, USA

ABSTRACT

Deep percolation of water is consistently identified as critical to the assessments of the performance of the proposed repository at Yucca Mountain, Nevada. In turn, simulations of deep percolation depend on appropriate surface boundary conditions. A series of 1D simulations of the near-surface environment, using a decade of measured hourly meteorological boundary conditions representative of the semi-arid Yucca Mountain area, is used to create a response surface for infiltration, which in turn is used to estimate the spatial variation of infiltration on a 6 km × 9 km grid at a 30 m × 30 m resolution. Two situations are considered, deep (semi-infinite) alluvium and shallow colluvium overlying a fracture continuum within an impermeable matrix. Sensitivities to meteorological factors are discussed for both situations. Based on the set of 1D simulations, formulae are presented relating annual average infiltration to hydraulic properties, annual average meteorologic inputs, and depth of colluvium. Infiltration is strongly affected by the depth of colluvium over the fractured bedrock, with infiltration decreasing with depth of cover but becoming more sensitive to meteorologic changes. In order to incorporate the influence of colluvium depth on infiltration, a computational model to predict the spatial distribution of colluvial depth is presented. Based on simple relationships for annual-average meteorologic inputs and predicted colluvium distributions, annual average infiltration is calculated for each pixel in the grid. Highest infiltration is predicted to occur in areas of shallow colluvium with relatively cooler and wetter conditions, which are generally located along ridgetops, sideslopes, and headwaters of washes. The estimated annual average infiltration over the study area is most sensitive to the annual average precipitation, annual average temperature, and colluvium properties.

1 INTRODUCTION

Performance assessments of the high-level waste repository proposed to be sited at Yucca Mountain, Nevada, consistently identify moisture levels at the repository horizon and moisture fluxes passing through the repository horizon as being critical factors in the ability of the proposed repository to isolate waste from the environment (*Nuclear Regulatory Commission* [1992], *Nuclear Regulatory Commission* [1995], *Sandia National Laboratories* [1992], *Sandia National Laboratories* [1994], and *TRW* [1995]). As moisture fluxes at the repository level depend on the net moisture entering the mountain through infiltration, and as the climate at the Yucca Mountain site has changed and

will change over the time scales of regulatory interest, multiple lines of investigation must be used to bound the moisture fluxes expected at the repository, including measurements of current near-surface infiltration rates, measurements of deep moisture fluxes, numerical simulations of moisture redistribution, and indirect measurements of long-term infiltration rates.

The study presented here examines the spatial distribution of shallow infiltration at Yucca Mountain using numerical simulations. A motivation for the study is to provide insight into the spatial distribution of boundary conditions appropriate for simulations of the deep subsurface, and examine how these might be affected by hydraulic properties and climatic variation. The study abstracts detailed 1D simulations into a response surface for annual average infiltration (AAI) as a function of hydraulic properties, annual-average meteorologic inputs, and depth of surficial cover. Each input parameter to the response surface function is estimated for each pixel of a Digital Elevation Map (DEM) of the study area. Assuming that the response surface is appropriate over the scale of a DEM pixel, the set of input parameters at each pixel is used to predict AAI for the pixel. Using the average of AAI over the study area as a measure, the relative importance of each input parameter is assessed by examining the sensitivity of the measure to the input.

The overall approach of abstracting numerous detailed 1D simulations into a response function for AAI, then using the spatial distribution of the functional inputs to predict AAI, has the advantage of allowing extremely fast turnaround for screening exercises and sensitivity tests once the response function is available. For example, total computational time necessary to reproduce all analysis presented herein, aside from the detailed 1D simulations, is on the order of tens of minutes on a Sun Sparc-20 workstation. A detailed 1D simulation, for comparison, can take several hours to weeks to complete on the same workstation. Thus, the breadth of hypotheses regarding site conditions that can be tested using the response-surface approach is far wider than could be achieved with the same computational effort using 2D or 3D models. Nevertheless, the approach is questionable for regions where lateral flow strongly influences vertical flow, as may occur locally at Yucca Mountain (e.g., wash channels, at the foot of slopes).

There has been a fair amount of previous examination of infiltration in the Yucca Mountain region. *Flint and Flint* [1994] present a preliminary estimate of the spatial distribution of flux in the Yucca Mountain region, based primarily on measured matrix properties. Detailed modelling and conceptual exercises have been performed by *Hevesi and Flint* [1993], *Flint et al.* [1993], *Long and Childs* [1993], *Hevesi et al.* [1994], *Flint et al.* [1994], *Hudson et al.* [1994], and *Kwicklis et al.* [1994]. Modelling exercises have typically been limited to 1D, with 2D radial models being applied

to model particular infiltration experiments. A trend developing in the literature suggests that infiltration at Yucca Mountain is not dominated by flow in washes, where conventional wisdom might place peak infiltration rates, but rather is dominated by flow in the low-permeability but densely fractured welded tuffs cropping out at ridgetops and sideslopes. As the trend has developed, estimates of areally averaged infiltration have increased to as much as 25 mm/yr (roughly 15 percent of annual average precipitation), based on a network of neutron probes [*Flint et al.*, 1995].

Generally bedrock at Yucca Mountain is covered with a shallow skin of colluvium or alluvium, but scattered local patches of bare bedrock do occur, particularly along ridgetops and in the headwater portions of washes. In the current study, the shallow Yucca Mountain infiltration system is conceptualized as one of two limiting cases: (i) deep (effectively semi-infinite) alluvium, typical of washes; and (ii) a shallow skin of alluvium or colluvium, overlying a densely fractured welded bedrock idealized as a fracture continuum within an impermeable matrix. Recognizing that alluvium tends to be deeper than colluvium, although both materials can be characterized as porous media, the porous medium in the first limiting case will be referred to as alluvium and the overlying porous medium in the second limiting case will be referred to as colluvium. The analysis of *Stothoff* [1996] suggests that the transition between the limiting cases occurs with a depth of cover on the order of 5 to 10 m, and in the absence of lateral flow and fast pathways, evaporation alone in the semi-arid Yucca Mountain environment is sufficient to eliminate infiltration for depths of fractured-bedrock cover between the transition depth and roughly 25 to 50 cm.

Using a 1D nonisothermal simulator, BREATH [*Stothoff*, 1995], a series of simulations was run with various depths of alluvium, systematically varying meteorologic parameters. Based on these simulations, the relative importance of the meteorologic inputs is assessed in Section 2. Approximations for the functional dependence of infiltration to meteorologic parameters are presented in Sections 3 and 4. In Section 5, values of the annual-average meteorologic parameters are estimated using a DEM of the Yucca Mountain area, and sample distributions of annual average infiltration (AAI) are determined assuming that only the meteorologic parameters change in the entire Yucca Mountain area. In light of the sensitive dependence of infiltration on the depth of bedrock cover, the spatial distribution of the surface cover is critical to predicting the spatial distribution of AAI; thus, a simple steady-state colluvium/alluvium transport model, coupled with a weathering model, is proposed in Section 6 to estimate the spatial distribution of the thickness of the layer from the DEM. Finally, in Section 7, the spatial distribution of AAI is examined, and input parameters having the greatest impact on areal-average AAI are identified using first-order sensitivity coefficients.

2 SHALLOW INFILTRATION SIMULATIONS

By performing a sufficient number of simulations of the flow of moisture and energy in a 1D column representative of the shallow surface of Yucca Mountain, while changing hydraulic parameters and meteorologic inputs in a systematic way, it is possible to construct a response surface for the variation of AAI with the input values. In this section, the simulations used to construct the response surface are discussed.

The BREATH simulator used in the study considers the coupled flow of moisture and energy in a porous medium, and is described in detail by *Stothoff* [1995]. The sensitivity of net long-term infiltration estimates to hydraulic properties, using BREATH, was considered by *Stothoff* [1996]. Following the procedures in *Stothoff* [1996], two types of simulations are considered: (i) semi-infinite columns of alluvium, and (ii) columns of shallow colluvium overlying a semi-infinite fracture continuum. In both cases, the semi-infinite behavior is approximated by using columns deep enough that the bottom boundary conditions have minimal impact on the estimated net infiltrations. A domain of thirty meters in depth is assumed to be sufficient to achieve this goal for the hydraulic and thermal properties considered.

All simulations presented in this paper use similar boundary conditions. At the bottom of the column, the gradients of saturation and temperature are assumed to be zero, allowing gravity drainage of water and advective losses of energy. At the top boundary of the column, the simulator is presented with 10 years of meteorological inputs, based on hourly readings from the Desert Rock, NV, National Weather Service meteorologic station located approximately 30 miles to the east of Yucca Mountain [*National Climatic Data Center*, 1994]; procedures for converting the National Weather Service readings into BREATH meteorological inputs are discussed by *Stothoff* [1996]. The meteorological record runs from March 1, 1983, through February 28, 1993. The decade of weather is repeated until the effects of the initial conditions are eliminated, so that the net flux over the decade is the same at each node; centuries may be required in low-AAI cases. All reported results are for the last simulated decade. One decade may be too short of a time period to capture the full range of precipitation events in a statistically robust way; however, considerable insight can be gained on the behavior that might be expected from the columns over longer periods of time.

Whenever precipitation exceeds infiltration, the excess is assumed to run off; overland flow is not considered further. Within 24 hours of a precipitation event, hourly meteorological readings are used; otherwise, moving monthly average readings are used. Adaptive time stepping is used to

ensure mass balance, with a maximum time step of 1 hour; during rainfall events, a single hour may take several hundred time steps.

In order to examine the impact on AAI in deep alluvium, two homogeneous alluvium columns are considered, using a high-permeability (intrinsic permeability $k = 10^{-5}$ cm^2) and a medium-permeability ($k = 10^{-8}$ cm^2) alluvium. For each column considered, porosity is 0.3, van Genuchten m is 0.2, and van Genuchten α is 1×10^{-3} Pa^{-1}. The 30-m column is discretized with 51 nodes, with a top element of 2 cm and each successive element increasing in length by 10 percent. Both alluvium cases were considered by *Stothoff* [1996], who found that for a similar semi-infinite column with all parameters held constant aside from permeability, as permeability increases from 10^{-5} cm^2 to 10^{-10} cm^2, AAI increases to a peak value with permeability at roughly 10^{-8}, then drops precipitously to essentially zero with permeability at 10^{-10} cm^2. Much higher net infiltration occurs for the medium-permeability alluvium than for the high-permeability alluvium due to reduced evaporation.

The base-case simulation for each alluvium uses the Desert Rock meteorological record directly. In order to identify first-order sensitivities to inputs, an additional pair of simulations is run for each column, systematically perturbing one of the inputs about the base-case value. *Stothoff* [1996] considered the systematic perturbation of hydraulic properties; the current study examines the perturbation of meteorologic inputs.

The long-term net infiltration rate resulting from each simulation is plotted in Figure 1, where the perturbation for most weather parameters is obtained by uniformly scaling each hourly value for the parameter. Temperatures, however, are perturbed by adding a constant value to all hourly temperature values. Relative changes in AAI for the same perturbation in the meteorologic input parameter are roughly twice as great in the low-AAI (high-permeability) column than in the high-AAI (medium-permeability) column. In Figure 2a, AAI for the sets of simulations are plotted as a function of the annual average saturation (AAS) below the wetting pulse perturbation depth. The strong correlation between AAI and AAS is due to the rather low variation in saturation about the mean value at depth, so that essentially steady-state gravity drainage is occurring at the bottom of the column. Under unsaturated gravity-drainage conditions, the relative permeability function provides a direct relationship between flux and saturation, explaining the strong correlation between AAI and AAS in Figure 2a.

The simulations shown in Figure 2a are plotted again in Figure 2b, except that AAI is divided by the square root of permeability and each AAS is normalized by the corresponding base-case

AAS. The simple scaling transformation is fairly successful in aligning the two cases, with both sets having equivalent slopes and with the ratio between scaled base-case AAI values about 10 percent of the ratio between base-case AAI values. Scaling by $k^{0.55}$ (rather than $k^{0.5}$) eliminates the gap in scaled AAI between the two sets, but there is little physical justification for the alternative scaling.

Meteorological factors have less impact on AAI in deep alluvium than do the hydraulic properties examined by *Stothoff* [1996], so that it can be concluded that identifying the hydraulic properties of deep alluvium is overall more significant to identifying AAI at Yucca Mountain. Nevertheless, systematic trends in the meteorologic variables (i.e., due to elevation variation or due to climatic change) can yield systematic variation in AAI. Elevation variation results in systematic variability in annual-average precipitation (AAP), annual-average temperature (AAT), and annual-average vapor density (AAV), while topographic effects result in systematic variability in incident shortwave radiation. Significant variation in both AAP and AAT should occur due to climatic change, with perhaps some change in AAV and cloud cover (with concommittant impact on longwave radiation) as well. Of these factors, AAP and AAT would appear to have the most significant impacts on the spatial distribution of AAI, a point that will be demonstrated in Section 5.

Although the response of AAI to meteorologic inputs is of interest in deep alluvium, the case of a shallow layer of alluvium or colluvium overlying a fractured bedrock is of greater interest, as only about 30 percent of the Yucca Mountain surface area is mapped as alluvium [*Scott and Bonk*, 1984]. Based on the observation that AAP and AAT appear to have the most significant impact on AAI, a detailed investigation of the impact of AAP and AAT on AAI in a colluvium/fracture system was performed. The high-infiltration alluvium used in the deep-alluvium simulations is also used in each of the colluvium/fracture simulations. The fracture continuum is characterized by an intrinsic permeability of 10^{-2} cm^2, porosity of 0.001, van Genuchten m of 0.7, and van Genuchten α of 0.1 Pa^{-1}. It is assumed that the welded-tuff matrix below the colluvium is essentially impermeable on the time scales of a precipitation event and thus does not interact significantly with the fractures. Fracture properties considered here are based on the range of parameters reported by *Schenker et al.* [1995], and are representative of both the Tiva Canyon and the Topopah Springs welded tuffs. *Stothoff* [1996] found that the fracture properties do not materially impact simulated infiltration rates as long as some small percentage of the fractures are open. The combination of alluvial and fracture properties is identical to the hydraulic-property base case considered by *Stothoff* [1996], and yields relatively high rates of infiltration. The base-case meteorologic input considered here was used for all simulations presented by *Stothoff* [1996].

Colluvium thicknesses of 2 cm, 5 cm, and 15 cm are considered, with a total column depth of 30 m. Although deeper colluvium may yield significant AAI, a decade is too short a period for the weather sequence to generate enough large wetting pulses (i.e., 10-yr, 100-yr storms) able to reach the colluvium/fracture interface to provide useful sensitivities. Aside from considering a two-layer system, all other procedures remain the same as when considering the deep-alluvium case; however, all simulations respond quickly enough that the effects of the initial conditions are eliminated within the first decade and the second decade can be used to determine AAI.

For every meteorology-sensitivity simulation presented here, at least 20 elements are used for the colluvium layer and 30 elements for the fracture layer. Elements at the surface and at the interface are on the order of 1 mm in length. The refinement level is considerably finer than used by *Stothoff* [1996] to identify sensitivities to hydraulic properties, as the sensitivity of AAI to meteorologic influences is much smaller than the sensitivity to hydraulic properties.

A range of precipitation and temperature variation sufficient to account for climatic variation was examined. For the 15-cm set, 9 cases were examined, including all combinations of AAP multipliers of 0.67, 1, and 1.5, with AAT shifts of -5, 0, and 5 °C. For both of the 2-cm and 5-cm sets, an additional 8 cases were examined by including all combinations of AAP multipliers of 0.5, 1, and 2, with AAT shifts of -10, 0, and 10 °C. The set of simulations is presented in Figure 3, where the sensitivity cases for each depth are shown by plotting AAI versus AAS as nested boxes. The AAI/AAS pair for each simulation is denoted by a symbol. Relatively horizontal lines represent unchanging AAP, with cooler conditions to the right; relatively vertical lines represent unchanging AAT, with wetter conditions to the top. For the 15-cm set, some of the hot and dry simulations yielded no AAI within simulator roundoff-error limits; these are not shown.

There is an obvious trend for decreasing AAI with increasing depth of cover in Figure 3; *Stothoff* [1996] found a similar trend for each of 17 combinations of colluvium and fracture hydraulic properties. If the relative perturbations were unaffected by depth, AAP, and AAT, the nested boxes would be essentially parallelopiped in shape and identical in size for each depth. As identical perturbations yield wider spreads in AAI as depths increase, AAI is demonstrated to be relatively more sensitive to both AAP and AAT as colluvium depths increase. In addition, as cooler or wetter conditions prevail, relative sensitivity of AAI to meteorologic inputs decreases. Thus, as AAI increases the relative sensitivity to meteorologic perturbations decreases, in common with the deep-alluvium simulations.

3 RESPONSE FUNCTIONS FOR DEEP ALLUVIUM

By performing a sufficient number of simulations of the flow of moisture and energy in a 1D column representative of the shallow surface of Yucca Mountain, changing hydraulic parameters and meteorologic inputs in a systematic way, it is possible to build up a response surface for the response of AAI to the input values. In this section, the response of AAI in deep alluvium is abstracted into simple formulae. Based on simulations presented by *Stothoff* [1996], the response of AAI to hydraulic properties is abstracted. With the hydraulic-property abstraction in hand, the influence of meteorologic inputs on AAI is abstracted. Using the response surfaces, it is possible to estimate the behavior of AAI at selected locations in the Yucca Mountain area.

Stothoff [1996] demonstrated that there are two distinct behaviors for AAI in deep alluvium, depending on the value for permeability. In low-permeability media, there is essentially no annual average infiltration. Significant numbers of wetting events have rainfall rates too large for the ground to accept, runoff often occurs, and evaporation is able to reclaim the small amount of AAP that actually enters the ground. In high-permeability media, there is a trend towards decreasing AAI with increasing permeability. All precipitation is accepted into the ground; however, evaporation becomes more effective with increasing permeability, leaving less moisture for net infiltration. The permeability yielding greatest AAI is roughly 10^{-8} cm^2, for which most events are accepted by the medium but some of the largest storms generate runoff. The largest-AAI permeability is characteristic of silty sands or fine clean sands *Freeze and Cherry* [1979]. There is a rapid dropoff in AAI as permeability decreases from the largest-AAI permeability; media only one to two orders of magnitude lower in permeability fall into the zero-infiltration category.

Characterizing the behavior of a low-permeability medium is quite straightforward; below a cutoff permeability, any imbibing water is removed by evaporation, so that AAI is zero. High-permeability media are of greater interest, as there are quantifiable trends in the behavior of AAI. Through a process of trial and error, a first-order relationship between AAI and the hydraulic properties was derived,

$$\log_{10}\left(\frac{AAI}{AAP}k^{1/2}\right) = \alpha_0 + \alpha_1\left[\left(\frac{m}{m_0}\right)^2 - 1\right] + \alpha_2\left[\left(\frac{P_0}{P}\right)^{1/2} - 1\right] + \alpha_3\left[\left(\frac{\varepsilon}{\varepsilon_0}\right) - 1\right], \qquad (1)$$

where k is intrinsic permeability, m is van Genuchten $m = 1 - 1/n$, P is bubbling pressure (the reciprocal of van Genuchten α in the units used here), ε is porosity, a subscript 0 represents a reference value for the parameter ($m_0 = 0.2$, $P_0 = 2000$ Pa, and $\varepsilon_0 = 0.3$), and the α values are hydraulic-parameter sensitivity constants.

Least-squares regression identified the α constants, using the AAI values from the 28 simulations with $k > 10^{-9}$ cm^2, finding that $\alpha_0 = -4.1$, $\alpha_1 = 0.61$, $\alpha_2 = 1.7$, and $\alpha_3 = -0.91$. The simulated values of AAI are compared with the first-order relationship in Figure 4. It can be seen that the fit between the simulated and the approximated values is quite good for the van Genuchten m value and the porosity; the simulations yield noisy values of AAI for the bubbling pressure, but the trend appears to be captured reasonably well.

As AAI is typically much less in deep alluvium than in shallow colluvium, and simulations take much longer to complete due to the long response time for deep alluvium, the issue of sensitivity to meteorologic input is only examined in detail for the shallow-colluvium case. Nevertheless, based on the simulations presented in Figure 2, some observations can be drawn about the observed response of AAI to meteorologic inputs in deep alluvium. For the two k values considered, the relationship

$$\log_{10}\left(\frac{AAI}{AAP}k^{1/2}\right) = \beta_0 - \beta_1 \log_{10}\left(\frac{AAL}{AAL_0}\right) + \beta_2 f_P\left[\log_{10}\left(\frac{AAP}{AAP_0}\right)\right] - \beta_3 f_T\left(\frac{AAT}{AAT_0} - 1\right) + \beta_4\left[\left(\frac{AAV}{AAV_0}\right)^2 - 1\right] - \beta_5 \log_{10}\left(\frac{AAW}{AAW_0}\right) \qquad (2)$$

appears to fit the simulated values reasonably well, where AAL is annual average longwave radiation, AAW is annual average windspeed, $f_P[\log_{10}(AAP/AAP_0)]$ is a quadratic or cubic function, $f_T(AAT/AAT_0)$ is a linear or quadratic function, and the β_i are fitting coefficients. Base-case annual-average values are used for normalizing: (i) $AAL_0 = 320$ W/m^2, (ii) $AAP_0 = 163$ mm/yr, (iii) $AAT_0 = 290$ K, (iv) $AAV_0 = 4.5 \times 10^{-6}$ gm/cm^3, and (v) $AAW_0 = 4.1$ m/s. For reference, the simultaneously determined least-square fit β values for the low-infiltration medium are shown in Table 1. Coefficients β_2 and β_3 in Table 1 are based on the assumption that both f_P and f_T are linear functions. Each of the β values scaling a meteorologic input is larger in magnitude for the high-permeability (low-infiltration) alluvium than for the medium-permeability (high-infiltration) alluvium, demonstrating an increased sensitivity to meteorologic input paramters as evaporation becomes more dominant. Unfortunately, the coefficients do not scale uniformly with changing permeability. Considerable additional work is required to verify the precise nature of the relationships between hydraulic properties, meteorologic inputs, and AAI in deep alluvium.

In order to estimate AAI using Equations 1 and 2, Equation 1 is used both to provide a first estimate for AAI and to estimate β_0 in Equation 2 (β_0 is set equal to the right-hand side of Equation 1). The remaining β coefficients in Equation 2 are obtained by using $\log_{10}(AAI)$ to linearly interpolate between the two β sets, and a corrected value of AAI is obtained using Equation 2. If k is smaller than 10^{-9} cm^2, it is assumed that $AAI = 0$. At the Yucca Mountain site, the procedure breaks down in the range of 10^{-8} through 10^{-9} cm^2.

4 RESPONSE FUNCTIONS FOR A COLLUVIUM/FRACTURE SYSTEM

For the purposes of estimating the spatial distribution of AAI using estimates of AAP, AAT, and colluvium depths as inputs, a functional relationship between these four variables is extremely useful. Through trial and error, a set of empirical relationships was derived for these variables. One relationship characterizes the decay of AAI with increasing colluvium depth and a second relationship uses corrections to the AAI/depth relationship to characterize the impact of AAP and AAT on AAI.

The first functional relationship accounts for the behavior of AAI due to the depth of colluvium. A set of 1D simulations that consider AAI as a function of alluvium hydraulic properties and depth were presented by *Stothoff* [1996], where each set varies one alluvium hydraulic property while keeping all other variables constant. Nine sets of simulations were presented by *Stothoff* [1996], with alluvium depths of 2, 5, 10, 15, and 25 cm. Each set shows that AAI decreases with increasing alluvium depth. Hypothesizing that a power law describes this behavior, the functional relationship for dimensionless infiltration ($I_D = AAI/AAP$) versus dimensionless depth ($B = \varepsilon b/b_r$) is in the form

$$\log_{10}(I_D/I_{D0}) \approx -C_I B^p, \tag{3}$$

where ε is porosity and b_r is a normalizing colluvium depth (taken as 2 cm in the following analysis). For a given value of p, the coefficients I_{D0} and C_I can be determined by regression.

Various approaches were examined for estimating p, based on minimizing the least-squares fit between the logarithms of the estimated and calculated I_D. A best-fit estimate for p is obtained by systematically varying p, obtaining the values for I_{D0} and C_I, and evaluating the residual between the data points and the approximation, until a value of p yielding the smallest residual is found. Each set of four or five simulations with identical hydraulic properties and different colluvium depths can be fit quite well with three fitting parameters, as might be expected. Best-fit estimates for p are quite variable, ranging from 0.25 through 1.09, although the least-square fits are relatively insensitive to p. Hypothesizing that a universal scaling behavior may be operative, so that p is identical for all hydraulic properties, a value for p was determined using all nine sets of simulations simultaneously but allowing separate values of I_{D0} and C_I to be determined for each set of simulations. Only simulations with AAI greater than 0.5 mm/yr were used in the regressions. The best fit value for p is 0.7073, suggesting that $p = \sqrt{1/2}$ may be an appropriate

scaling exponent. The regressed values for I_{D0} range from 0.641 through 1.21, and the values for C_I range from 0.562 through 1.02; the base-case values are 0.841 and 0.812, respectively. Interestingly, I_{D0} and C_I are numerically very similar, and have a correlation coefficient of 0.93. Parsimony of parameters suggests that I_{D0} and C_I should be assigned the same values, although there is little physical basis for this requirement. Enforcing parsimony yields values for I_{D0} ranging from 0.513 through 0.950.

A particularly clear example of the agreement between the simulations and the functional approximation is shown in Figure 5, which shows AAI as a function of colluvium depth for the cases where porosity is 0.2, 0.3, and 0.5. All three curves are generated using $I_{D0} = C_I = 0.7733$, where 0.7733 is the mean of the three values obtained by independently determining I_{D0} for the three porosity cases while assuming $I_{D0} = C_I$. Figure 5 is excellent justification both for including porosity in the dimensionless depth and using $I_{D0} = C_I$ for each material set. The match between simulation and approximation is of similar quality for the other colluvium-property cases.

The value of I_{D0} incorporates the influence of both colluvium and fracture hydraulic properties. The set of base-case properties yields the lowest I_{D0} of the three colluvium-permeability cases, and the highest I_{D0} of the three colluvium-van Genuchten m cases, so no clear trend is apparent for either case. However, I_{D0} appears to be linearly dependent on colluvium bubbling pressure, with I_{D0} increasing with increasing bubbling pressure. The base case has a colluvium permeability that yields particularly high AAI values; accordingly, it seems reasonable to hypothesize that different functional forms may exist for permeabilities greater than the base case and for permeabilities less than the base case. Further work is required to resolve the functional relationship between I_{D0} and hydraulic parameters.

The effect of changes in AAP and AAT on AAI can be directly investigated by dividing I_D by I_O, where I_O is the I_D for the simulations using base-case meteorologic input parameters. By plotting I_D/I_O as a function of AAP, AAT, and colluvium depth, the trend of increasing sensitivity to meteorologic input parameters with increasing evaporation, identified in the deep alluvium analysis, is again observed with the colluvium/fracture system. Three trends support this observation: (i) I_D/I_O becomes much more sensitive to changes in AAP as AAT increases, (ii) I_D/I_O becomes much more sensitive to changes in AAT as AAP decreases, and (iii) I_D/I_O becomes more sensitive to AAP and AAT with increasing colluvium depth. A modified dimensionless parameter, H, was found to account for most of the depth-dependency, where

$$\log_{10}(H) = B^{-r} \log_{10}(I_D/I_O). \tag{4}$$

A range of values around 0.7 for the r fitting parameter scaled the data reasonably well. The p and r exponents are parsimoniously assumed to have the same numerical value, particularly since there is insufficient data to clearly distinguish them. Both p and r are assigned the same value of $\sqrt{1/2}$.

A further functional relationship adjusts H to account for the deviation from the base-case meteorological input parameters. Plots of H as a function of T and M, where T is the relative change in AAT [$T = (AAT - AAT_0)/AAT_0$] and M is the change in the base-10 log of the AAP multiplier [$M = \log_{10}(AAP/AAP_0)$], suggest that H varies exponentially with both parameters. Accordingly, a new variable $J = \log_{10}(H)$ was defined. J values were calculated for each combination of T, M, and colluvium depth, then averaged over all colluvium depths to yield a set of mean $\overline{J}$ values. Only J values resulting from simulations with significant net infiltration were used in calculating $\overline{J}$. Finally, a bicubic function, J_{fit}, of T and M was regressed to $\overline{J}$,

$$J_{fit}(T,M) = j_0 + j_1 M + j_2 T + j_3 M^2 + j_4 MT + j_5 T^2 + j_6 M^3 + j_7 M^2 T + j_8 MT^2 + j_9 T^3, \quad (5)$$

where values for the regressed coefficients, j_i, are shown in Table 2. Interestingly, the magnitude of the ratio of j_1 to j_2 is of the same order as the ratio of β_2 to β_3 (i.e., 0.13 for j_1/j_2; 0.20 and 0.13 for β_2/β_3 in high-infiltration and low-infiltration media, respectively) suggesting that corrections to AAI due to meteorologic influences may be closely related for the deep-alluvium and colluvium/fracture systems and suitably scaled deep-alluvium corrections for the remaining meteorologic influences might be added on to J_{fit}. It is reasonable to assume that J_{fit} is also a function of hydraulic properties, although this cannot be justified based on the current work. It would not be surprising to find that J_{fit} is scaled by C_I. Accordingly, a new variable is defined, $J_0 = -J_{fit}/C_I$, where the minus sign is used for convenience.

The impact of the functional approximations can be seen in Figure 6, in which AAI calculated in a 1D simulation is plotted against the corresponding approximated AAI. In order to compare only climatic influences, all AAI values are normalized by the base-case AAI for the corresponding colluvium depth. The approximation provides very good explanatory power; the maximum deviation between the simulated and approximated AAI is 0.82 percent of the range of simulated AAI. It is expected that longer periods of meteorological input would improve the approximation, by providing a better statistical sample of wetting events.

Putting together the shallow-colluvium functional relationships, the parsimonious fitted response of AAI to colluvium depth and meteorologic factors reduces to

$$\log_{10}[AAI(b,T,M)/AAP] = \log_{10}(I_{D0}) - I_{D0} B^{\sqrt{1/2}}(1 + J_0(T,M)). \quad (6)$$

This approximation is used to calculate the response of AAI to meteorologic factors in subsequent sections.

5 IMPACT OF METEOROLOGY ON SPATIAL DISTRIBUTIONS OF INFILTRATION

In order to transfer the sensitivity information to a spatial distribution of infiltration, the spatial distribution of the meteorological parameters is required. Simple models are used here to estimate spatial distributions of meteorological factors. Presuming that long-wave radiation is essentially constant over Yucca Mountain and the sensitivity of AAI to long-wave radiation is relatively small, and noting that AAI is relatively insensitive to windspeed, these two factors are neglected in the current analysis. AAP is estimated by an exponential expression regressed by *Hevesi et al.* [1992], based on cokriged elevation and AAP for 42 stations in southwestern Nevada.

$$AAP = \exp(4.26 + 0.000646Z) \tag{7}$$

The authors are not aware of a similar regression for AAT or AAV, so the Desert Rock station and a central Nevada meteorological station at elevation 7200 feet [*McKinley and Oliver*, 1994] are used to estimate AAT and AAV, assuming temperature decreases linearly and vapor density decreases exponentially with elevation. The formulae used to estimate elevation-dependent distributions are:

$$AAT = 25.83 - 0.00840Z \tag{8}$$

$$AAV = \exp(-11.96 - 0.000341Z) \tag{9}$$

where Z is ground-surface elevation in meters, AAP is in mm/yr, AAT is in °C, and AAV is in gm/cm^3. A typical lapse rate for temperature is on the order of 5 to 6 °C/km [*Fairbridge*, 1967]; the somewhat higher rate of 8.4 °C/km used here can be attributed to the aridity of the southern Great Basin. The elevation of the ground surface is obtained from a 6 km E-W × 9 km N-S DEM of the subregional area, with a grid resolution of 30 m × 30 m. The DEM has a minimum elevation of 1110 m and maximum elevation of 1752 m (elevation over the proposed repository footprint ranges from roughly 1250 to 1500 m). AAP ranges from 145 mm/yr to 220 mm/yr, AAT ranges from 11.1 °C to 16.5 °C, and AAV ranges from 3.17×10^{-6} gm/cm^3 to 2.59×10^{-6} gm/cm^3 over the DEM range in elevation. Corresponding values from the Desert Rock data (elevation about 1000 m) are 163 mm/yr, 17.4 °C, and 4.52×10^{-6} gm/cm^3; the decade represented by the Desert Rock data is somewhat wetter than average.

Modification of the base-case AAI by solar radiation is estimated by calculating the north-south and east-west rotations of the ground surface, and interpolating within a table obtained from simulations using solar loads appropriate to surface rotations 30 degrees to the east, west, north, and south. Note that all simulations treat runoff identically, regardless of the solar loading. Although average ground temperatures may be several degrees Celsius warmer or colder than the base case due to solar aspect, surprisingly the calculated net infiltrations are almost insensitive to solar aspect. For a semi-infinite column of medium-permeability alluvium, the ratio of infiltration for a rotated-aspect solar load to infiltration for the unrotated solar load is 1, 0.845, 0.897, and 0.759 for rotations 30 degrees to the east, west, north, and south, respectively. For comparison, the corresponding ratios are 1.032, 1.032, 1.280, and 0.857 for the high-permeability alluvium. For the high-infiltration case, solar loading near the time of precipitation appears to be important, insofar as the solar load for the east and west rotations are identical but different AAI is obtained for the two cases. There may be a bias in the time of day precipitation events occur that enhances evaporation from the east-rotation case. For the low-infiltration medium, solar loading may be significant for longer periods of time and causes a wider spread in AAI. It would be reasonable to assume that shadowing effects, in which the sun is blocked by ridges for part of the day, will have additional impacts on infiltration of similar magnitude. In general, north-facing slopes would be expected to have more infiltration than south-facing slopes, by perhaps a factor of 50 percent based on the ratio of north-facing AAI to south-facing AAI. Relative to uncertainties in hydraulic properties and alluvium depths, solar radiation has a relatively insignificant impact on infiltration. Although direct solar-loading effects on infiltration are not large, indirect effects may be significant, as vegetation and weathering rates are also dependent on solar loading.

The impact of the spatial distribution of the meteorologic input parameters on AAI is examined in a straightforward manner for both deep-alluvium cases. Based on Figures 1 and 2, it is assumed that infiltration varies log-linearly with perturbations in meteorologic parameters. It is further assumed that the effects of varying any meteorologic input parameter are independent of the remaining meteorologic input parameters, so that the input parameters can be considered separately. A separate tabular response function is formed for each meteorologic input parameter, using the AAI values for the set of simulations presented in Figure 1 divided by the corresponding base-case AAI. Given the value of a meteorologic parameter within a pixel, the AAI/base-case AAI ratio is determined by lookup. The ratios for the four meteorologic influences are multiplied, and the resulting scaled AAI is forced to be positive and no more than AAP.

An example spatial distribution of the AAI/base-case AAI ratio is shown in Figure 7, in which it is assumed that the entire region is uniformly covered with semi-infinite high-infiltration alluvium and all variation is due solely to the spatial distribution of the four meteorological factors. The maximum AAI is about 5 times the minimum AAI for this case; over the repository footprint the ratio is roughly two. The distribution of AAI for the high-permeability alluvium is essentially identical, except that the relative range of AAI, 14, is considerably larger (consistent with Figure 2). The impact for each of the four factors is presented both individually and as a group in Table 3. The individual impact of each meteorological input parameter is estimated by assuming that each pixel has the base-case value for the remaining input parameters. AAP and AAT are the meteorologic input parameters with the largest impact on the spatial distribution of AAI at the Yucca Mountain scale, both acting to increase infiltration with elevation. AAV has a numerically smaller impact, but acts to decrease AAI with increasing elevation. Solar radiation also has minor impact on the distribution of AAI. The increase in AAI spread as permeability increases primarily arises from the evaporation-affecting parameters (AAT, AAV, and solar radiation). Note that variation in AAP causes the bulk of the spread in AAI for the lower-evaporation material; for the higher-evaporation material, variation in AAT causes the bulk of the AAI spread.

6 ESTIMATING ALLUVIAL DEPTH DISTRIBUTIONS

It was demonstrated by *Stothoff* [1996] that the depth of shallow colluvial cover over a fractured bedrock can have a profound impact on simulated net long-term infiltration. For example, simulations including 2 cm of colluvium covering a fracture continuum indicate 1/3 of annual-average precipitation may become net infiltration, while 50 cm of the same alluvium cover yields essentially no net infiltration. For relatively low-permeability colluvium, colluvium porosity is the hydraulic property that arguably has the most significant impact on simulated net infiltration. Other hydraulic properties typically have relatively little effect for cases with less than 50 cm of cover. *Stothoff* [1996] found that simulated infiltration rates are not sensitive to fracture properties, as long as a few fractures are open and available to conduct flow.

The proposed repository footprint underlies several types of surface terrain, each with distinct infiltration characteristics. Bedrock is entirely volcanic in origin, with much of the surface exposures consisting of ash-fall tuff with various degrees of welding. The highest zone within the footprint is the north-south ridge called Yucca Crest. A resistant, relatively unfractured caprock in the Tiva Canyon Member forms a crest with relatively shallow slopes to the east and slopes of up to 50

degrees to the west. The Tiva Canyon caprock forms the top of at least part of most of the ridges within a few km of the Yucca Mountain area. The caprock breaks into boulders upon weathering, up to several meters in length, which can roll hundreds of meters into Solitario Canyon, west of the crest. At the extreme crest, bare-rock outcrops can form up to 3/4 of the surface, with pockets of fine-grained colluvium ranging from 0 to 15 cm in depth. Colluvium also is present in gaps between outcrops and boulders, thus runoff is able to concentrate on a local scale.

The lower portion of the Tiva Canyon Member lies immediately below the caprock. The vast majority of the repository footprint is below surface outcrops of this densely fractured, welded unit. The lower Tiva Canyon Member is less resistant than the caprock, typically breaking along cooling joints and fractures into chunks that are less than 50 cm in dimension. Calcite fracture fillings are present in portions of this layer, particularly in faulted zones. Along ridgetops with the lower member exposed, pockets of fine colluvium have depths on the order of 10 to 20 cm, gradually increasing in depth with distance downslope. Generally the bases of the slopes at wash channels have colluvium at most slightly more than a meter in depth.

Remnant alluvial terraces exist in washes in the eastern part of the footprint that may be 4 m and more in depth, with wash channels incised into the alluvium for various depths up to a few meters. Proceeding from west to east, wash bottoms widen from less than a meter to 100s of meters. In the narrowest channels and some upstream slopes, bare rock is exposed, with bare fractured bedrock present to the center of the footprint in some channels. As wash channels widen past 1 to 2 m, alluvial deposits begin to completely cover bedrock.

In the extreme western portion of the footprint, exposures of underlying units are found on the eastern flanks of Solitario Canyon. Immediately underneath the Tiva Canyon Member lies the Paintbrush Member, comprising a series of non- to partially welded ash-fall tuff layers. The Paintbrush Member tuffs are relatively easily eroded, with porosities up to 50 percent, and total thickness on the order of 40 m. Below the Paintbrush Member lies the welded and densely fractured Topopah Spring Member, which is the layer in which the repository would be located. The Topopah Spring Member is quite similar to the lower Tiva Canyon Member.

Colluvium and alluvium in the Yucca Mountain area are composed of fine sands mixed with coarser rock shards and boulders, with the largest rock fragments decreasing in size from higher to lower elevations. At the highest elevations and on slopes steeper than the angle of repose, the mixture is essentially fine colluvium distributed on and around outcrops and large boulders. In the

shallowest colluvium, where net infiltration should be greatest, the largest materials are much larger than average colluvium depths, so that assigning representative depths and porosities is fraught with difficulty. Estimating infiltration is exacerbated by the nonlinear response of infiltration to colluvium depth and porosity, so that using an areal average over a grid cell for both depth and porosity, in order to estimate infiltration, does not necessarily yield estimates that are equivalent to the areal average of infiltration over the grid cell.

Since infiltration is sensitively dependent on the distribution of shallow colluvium, and a detailed map of shallow colluvium depth is not available and may be extremely difficult to measure, an alternative approach for estimating colluvium depth was followed here. A simple mechanistic model of combined colluvium and alluvium erosion and redistribution was created, using a DEM for the underlying elevation controls, in order to estimate colluvium depths. The model takes into account erosion and sediment transport due to water movement, as well as soil creep and passive degradation. As a first step, the model only accounts for one generic particle size, rather than considering a distribution of particle sizes. The model does not directly calculate erosion due to rain splash or long-range transport due to gravity (i.e., boulders rolling downhill). For simplicity of terminology, colluvium and alluvium will be collectively refered to as alluvium in the model description.

In the current implementation, spatial variability in alluvium depths arises solely from the variability in surface elevation; all erosion-balance parameters are assumed constant in space. The alluvium-balance mathematical model generally follows *Beaumont et al.* [1992], with the overland flow and erosion models based upon work presented by *Woolhiser et al.* [1990].

Three equilibrium balance equations are solved to calculate the equilibrium depth of alluvium over the Yucca Mountain region; (i) an overall alluvium mass balance, (ii) a sediment mass balance, and (iii) a hydraulic mass balance or stream-flow model. The overall mass balance for alluvium, the first equation, is

$$\nabla \cdot \mathbf{q}_{alluv} + Q_{wea} + \overline{Q_{str}} = 0, \tag{10}$$

where $\mathbf{q}_{alluv}$ is the flux of alluvium, Q_{wea} is the source of alluvium due to weathering, and $\overline{Q_{str}}$ is the time-averaged flux due to stream action. The erosion-balance model assumes that all processes are at equilibrium. Thus, the stream-flow model assumes that a representative spatially uniform rainfall rate is applied over the entire mountain, and the resulting equilibrium hydraulic flux distribution is used to calculate equilibrium sediment transport. As streamflow is actually highly episodic at

Yucca Mountain, the equilibrium sediment-transport velocities and erosion/deposition rates must be adjusted to account for the time with no streamflow. Time averaged stream-action flux is approximated here by

$$\overline{Q_{str}} \approx F_{str} Q_{str}, \tag{11}$$

where F_{str} is the fraction of time stream flow occurs. The procedure is likely to under-represent the time average in headwater and overland-flow areas, and over-represent the time average in deep washes and downstream areas.

Flux of alluvium, other than through sediment transport, is assumed to occur through creep and is gravity-driven,

$$\mathbf{q}_{alluv} = -Kb\nabla Z, \tag{12}$$

where b is the depth of alluvium, Z is the ground surface elevation, and K is a creep conductance (assumed spatially constant here). The alluvium-flux term is similar to the short-range transport model used by *Beaumont et al.* [1992], except that here b varies with time and Z is constant, while in the *Beaumont et al.* [1992] application, b is assumed constant and Z is allowed to vary over time.

A simple source term representing weathering is used here. It is assumed that alluvium protects the bedrock from weathering, so that weathering decreases exponentially with alluvial depth:

$$Q_{wea} = Q_0 \exp(-b/b_0) \tag{13}$$

where Q_0 is the source strength, and b_0 represents a weathering-protection alluvium depth. The weathering model has two fitting parameters, Q_0 and b_0, which can be used to match observed alluvium depths.

Erosion and deposition through stream action is calculated using the second equilibrium balance equation, a sediment-balance equation,

$$\nabla \cdot c_s \mathbf{q}_w - Q_{str} = 0, \tag{14}$$

where c_s is the concentration of the sediment in water and $\mathbf{q}_w$ is the flux of water. Following standard practices in the literature (e.g., *Woolhiser et al.* [1990]), a simple kinetic rate law is used to characterize erosion and deposition,

$$Q_{str} = C_g(c_s - c_{eq}), \tag{15}$$

where c_{eq} is the equilibrium sediment concentration for a reach along a stream bed and C_g is an equilibrium constant.

Numerous equilibrium sediment concentration capacity relationships exist in the literature (e.g., *Yang* [1973], *Kilinc and Richardson* [1973], *Ackers and White* [1973], *Yalin* [1963]). A particularly simple relationship is used herein [*Meyer and Wischmeier*, 1969], based on tractive force:

$$c_{eq} = C_s \frac{v^4}{h}, \tag{16}$$

where C_s is a constant, v is water velocity, and h is hydraulic depth.

For erosion, C_g is a constant describing the erodibility of the alluvium or bedrock. For deposition ($c_s > c_{eq}$), C_g assumes that particles have fall velocities and drag characteristics similar to spheres [*Fair and Geyer*, 1954], and a coupled set of equations are used to calculate C_g:

$$v_s^2 = \frac{4}{3} \frac{g(S_s - 1)d}{C_D}, \tag{17}$$

$$C_D = \frac{24}{R} + \frac{3}{\sqrt{R}} + 0.34, \tag{18}$$

$$R = v_s d/\nu, \tag{19}$$

$$C_g = \frac{v_s}{h}\left(1 - \frac{c_{eq}}{c_s}\right), \tag{20}$$

where v_s is the particle settling velocity, g is the acceleration due to gravity, S_s is the particle specific gravity, d is the particle diameter, C_D is the drag coefficient, R is the Reynold's number, and ν is the kinematic viscosity.

The final equilibrium balance equation required to complete the alluvium-balance system is the water-balance equation,

$$\nabla \cdot \mathbf{q}_w + Q_{rain} = 0, \tag{21}$$

where Q_{rain} is the net rainfall. A standard practice in the literature is to use a kinematic-wave approximation for hydraulic flux in conjunction with the Manning hydraulic resistance law, so that (in metric units)

$$\mathbf{q}_w = \frac{S^{1/2} h^{5/3}}{n}, \tag{22}$$

where S is the slope and n is Manning's roughness coefficient.

Each of the three balance equations is solved using the same general finite-volume flow-routing approach. The DEM grid is discretized into square boxes, or nodes, with 1D connections to the

nearest eight nodes. Taking advantage of the hyperbolic nature of the equations by assuming that upstream variables uniquely determine fluxes to downstream nodes, the nodes in the grid can be processed in order from highest to lowest elevation in one pass.

The water-balance equation is solved independently of the sediment- and alluvium-balance equations. In the water-balance equation, each node is processed using the algebraic equation,

$$A_i q_{rain} + \sum_{j=up} \frac{w_{ij} h_j^{5/3}}{n} \left(\frac{Z_j - Z_i}{\Delta_{ij}} \right)^{1/2} - \sum_{j=down} \frac{w_{ij} h_i^{5/3}}{n} \left(\frac{Z_i - Z_j}{\Delta_{ij}} \right)^{1/2} = 0, \qquad (23)$$

where node i is the node being processed, node j is a neighboring node, A_i is the area associated with node i, q_{rain} is the rainfall rate minus infiltration, w_{ij} is the width of the 1D connection between nodes i and j, and Δ_{ij} is the distance between nodes i and j. Summing over upstream nodes is denoted by $j = up$, and summing over downstream nodes is denoted by $j = down$. On a square grid with constant node spacing Δ, w_{ij} is $\Delta/2$ for nearest-neighbor connections and $\sqrt{2}\Delta/3$ for diagonal connections.

The sediment- and alluvium-balance equations are solved simultaneously, by requiring that each nodal alluvium depth and sediment concentration is compatible with outflow from the node. The algebraic balance equations are:

$$\sum_{j=up} c_{sj} Q_{wij} - \sum_{j=down} c_{si} Q_{wij} + \frac{A_i}{8} \sum_{j=down} \overline{C_{gij}(c_{eqij} - c_{si})} = 0, \qquad (24)$$

$$\sum_{j=1}^{8} w_{ij} K_{ij} b_{up} \left(\frac{Z_j - Z_i}{\Delta_{ij}} \right) + A_i Q_0 \exp(-b_i/b_0) - \frac{A_i}{8} \sum_{j=down} \overline{C_{gij}(c_{eqij} - c_{si})} = 0, \qquad (25)$$

where b_{up} is the upstream alluvium depth. Alluvium depths are solved by bisection between a minimum depth of 0 m and a maximum depth (arbitrarily assumed to be 20 m here). The equilibrium sediment concentration is found during each bisection step.

The flow-routing approach works well when there are no local minima in the domain, so that there is a route from every node to the boundary. A physical local minimum cannot exist at equilibrium unless there is a physical mechanism for removing alluvium (e.g., wind transport). Typically, however, local minima are artifacts of the DEM resolution, as elevations are only reported to the nearest meter. Also, narrow features such as upstream wash channels, which are on the order of a meter wide, cannot be resolved with the 30-m DEM grid. About 0.5 percent of the nodes in the DEM are local minima, almost all occurring in wash bottoms but a few occurring along ridgetops.

For these minimum nodes, a preprocessing step was performed to eliminate artificial local minima, by artificially raising minima nodes at least 10 cm above the lowest of the surrounding nodes. The average change was 32 cm, with a maximum change of 2.19 m. A number of passes were required to eliminate multinode basins.

There are a total of 11 adjustable parameters in the set of coupled balance equations, The 11 parameters, and values found to result in reasonable predictions of colluvium depths, are shown in Table 4. As F_{str}, K, and Q_0 control the relative importance of stream processes, colluvial diffusion, and weathering. These three parameters are not completely independent, so scaling the three parameters by the same constant does not modify the predicted colluvium distribution. The distributions of hydraulic depth, sediment concentration, and colluvium depth shown in Figures 8 through 10, respectively, result from using the adjustable parameters in Table 4. A digitized outline of alluvium, as mapped by *Scott and Bonk* [1984], is shown in Figure 10 for reference. These distributions were generated by selecting representative parameters for the stream flow and sediment transport equations, then adjusting the alluvium parameters until the alluvium distribution was in reasonable agreement with the authors' observations of colluvium depths in trenches and other representative locations in the Yucca Mountain area.

The colluvium distribution illustrated in Figure 10 is quite plausibly rendered, on the whole. The model predicts average depths that are somewhat too large along crestlines and somewhat too shallow near the bottom of some of the side slopes, in part due to not imposing different weathering rates for the Tiva Canyon caprock and the lower Tiva Canyon Member. Headwaters of washes implausibly predict mixtures of deep alluvium and bare rock, due to the mismatch in resolution between the DEM and the wash channels; however, as the area with bare rock tends to be smaller than the grid size, this mixture does represent the infiltration distribution to some extent.

The biggest discrepancy between model predictions and the field observations is within the mapped alluvium outline, as evidenced by predictions of very shallow and very deep alluvium in adjacent pixels. The root of this discrepancy lies in the inherent dynamism of sediment transport processes in the deeper alluvium. Surface elevations vary over time as incised channels move around within deep alluvium, and it is unreasonable to expect that predictions based on equilibrium physics will behave properly when presented with a snapshot of such highly dynamic topography. The difficulty is only exacerbated by the 1-m vertical resolution of the DEM in the relatively horizontal wash bottoms.

Within the mapped alluvium outline, therefore, a post-processing step is performed to provide more realistic alluvium depths. An exponential relationship of alluvial depth to surface slope was determined by regression,

$$b = 47 \exp(-0.32s) \tag{26}$$

where s is the slope, in degrees, of the ground surface at the nearest grid point in the DEM. The coefficient of determination is 0.61 for the relationship, using information from 56 of the boreholes discussed by *Fernandez et al.* [1994]. Wherever the slope is less than 10 degrees within the *Scott and Bonk* [1984] alluvium outline, the alluvium depths were calculated using Equation 26; otherwise, the colluvium-routing model predictions are used. The effect of performing the post-processing is shown in Figure 11; this is the base-case alluvium distribution that will be used to estimate the spatial distribution of AAI at Yucca Mountain.

7 SPATIAL DISTRIBUTIONS OF INFILTRATION

Two issues are of particular interest when examining the spatial distribution of AAI. General trends in the spatial distribution of AAI are of interest (i.e., localized zones of high AAI), as is the sensitivity of the areal-average AAI to the various input parameters. The first issue is examined by using reasonable values for hydraulic properties, colluvium and alluvium depths, and meteorologic inputs, in conjunction with the regression formulae developed in previous sections, to predict the resultant distribution of AAI. The second issue is investigated by using first-order perturbations to the input parameters and examining the responses in the predicted areal-average AAI.

In order to estimate the spatial distribution of infiltration, the subregional area was subdivided into three classes: (i) deep alluvium, (ii) fractured welded bedrock overlain by colluvium, and (iii) nonwelded bedrock (PTn). Deep alluvium is classified as the area within the *Scott and Bonk* [1984] alluvium outline with ground slope less than 10 degrees, while the CNWRA 3D Geologic Framework Model (GFM) [*Stirewalt and Henderson*, 1995] was used to determine the exposure of bedded nonwelded tuffs (PTn). The remaining area was presumed to consist of welded-tuff bedrock overlain by colluvium. The classes are shown in Figure 12. The areas classified as deep alluvium and PTn are about 21 percent and 4 percent of the of the total subregional area, respectively.

Modeling AAI in PTn outcrop areas is problematic for several reasons: (i) the layer is thin enough to make the semi-infinite assumption questionable; (ii) bedding thicknesses are on the order

of meters, making the assumption of homogeneous properties questionable; (iii) roughly half of the measured permeabilities are less than 10^{-10} cm^2 [*Schenker et al.*, 1995], thus should yield zero *AAI*, but some measured permeabilities are in the range of 10^{-8} to 10^{-9} cm^2 and would be expected to yield significant and even quite large *AAI* in perhaps highly localized spots; and (iv) the other PTn hydraulic properties are highly variable. One would expect, therefore, that at least half of the outcrop area would yield zero *AAI*, while some of the remainder may yield *AAI* greater than deep-alluvium *AAI*. Due to the large uncertainty in PTn response, but relatively small exposure area, a simple, somewhat arbitrary, response function was assumed for the *AAI* in the PTn outcrop. PTn outcrops were modeled by assigning a fraction of the *AAP* as *AAI*. The base case used 10 percent of *AAP* for *AAI* in the PTn outcrops, regardless of colluvial cover; the sensitivity of areal-average *AAI* to the PTn was assessed using 0 and 20 percent of *AAP*.

An estimated spatial distribution for *AAI* is shown in Figure 13, based on the alluvium distribution in Figure 11 and the base-case deep-alluvium properties. The deep-alluvium properties are the same as the reference properties in Equation 1, with $k = 10^{-7}$ cm^2. The colluvium/fracture system is characterized using $I_{D0} = C_I = 0.7$, with a colluvium porosity of 0.2. The average *AAI* over the subregional area for this example is 15.0 mm/yr; within the 3 km E-W $\times$ 4 km N-S box surrounding the proposed repository footprint, the average *AAI* is 14.6 mm/yr. Within pixels classified as deep alluvium, PTn, and colluvium/fracture, average *AAI* is 2.4 mm/yr, 15.4 mm/yr, and 18.6 mm/yr, respectively. The estimated *AAI* distribution is useful for examining spatial patterns and sensitivities; however, it is anticipated that, even if all inputs were correctly estimated, the areal-average *AAI* would be significantly overestimated due to neglecting plant transpiration.

As shown in Figure 13, the largest *AAI*s tend to be on ridgetops and sideslopes. Part of this trend is due to enhancement of *AAI* through systematic meteorological variation; a larger part is due to progressive thinning of colluvial thickness with elevation. This point is demonstrated in Figure 14, which is a scatterplot drawn from the estimated *AAI* distribution in Figure 13. The strongest response is due to colluvium depth, which is the distribution of *AAI* decaying with depth to about 4 m. The distribution of *AAI* rising from about 5 m represents the deep alluvium. The horizontally oriented *AAI* distribution represents the influence of the PTn outcrop. There are also numerous pixels that have zero infiltration, not shown due to the logarithmic scaling. Meteorological factors cause the scatter in *AAI* observations. The relatively small amount of scatter is further indication that the response on *AAI* is dominated by hydraulic factors, rather than meteorological factors, on a pixel-by-pixel basis.

Little or no AAI is predicted in the wash bottoms. It is plausible to assume that there could be enhanced AAI at the foot of the sideslopes, due to overland flow of runoff; there may also be additional AAI within the intermittent stream channels within the washes. These effects cannot be easily quantified using the current model.

Using normalized sensitivity coefficients [*Sykes et al.*, 1985], the sensitivity S_k of areal-average AAI to generic parameter α_k,

$$S_k = \frac{\alpha_k}{AAI} \frac{\mathrm{d}AAI}{\mathrm{d}\alpha_k}, \tag{27}$$

can be examined. The sensitivity coefficients are calculated by using first-order derivatives between a high and low perturbation, normalized by a reference value. In general, sensitivity coefficients will change as the set of base input values change. Accordingly, sensitivity coefficients are calculated for a base-case AAI distribution and a set of alternate AAI distributions, where the alternate AAI distributions result from changing the base-case value for a single input parameter.

Values for the input parameters used to calculate sensitivity coefficients are shown in Table 5. For cases where alternate input-parameter values were used to examine sensitivity-coefficient variability, the alternate input values are shown as well as the resulting relative change in areal-average AAI. Sensitivity coefficients estimated using the perturbations in Table 5 are shown in Table 6. The sensitivity coefficients are for the entire region; the calculated areal-average AAI values within the 12 km^2 area centered on the repository footprint are generally within 25 percent of the regional values, so that sensitivity coefficients are quite similar.

An example may aid in interpreting Tables 5 and 6. Using k as the sample input parameter, the sensitivity coefficient for k using the base-case parameter set is found in column 4 of the first row. The base-case sensitivity parameter is evaluated using the relative values of AAI reported in columns 2 and 3, which result from evaluating areal-average AAI using the values of k in columns 2 and 4 of Table 5, respectively. The relative change in areal-average AAI resulting from using the alternate reference k value (column 6 of Table 5), is shown in column 5 of Table 5; note that all other input parameters are held at the base-case value. The sensitivity coefficient for k when the alternate k values are used (columns 5 through 7 of Table 5), is shown in column 5 of Table 6. Similarly, the sensitivity coefficient for k when the alternate set of ε_c values is used is shown in column 7 of Table 6.

As can be seen from Table 5, changing AAP and AAT individually by amounts that might be seen in a pluvial period results in relative increases in areal-average AAI of 3.1 and 2.0 for the

base-case set of hydraulic properties. For comparison, simultaneous changing both two factors by the amount shown in the table results in a relative increase of 4.9.

Interestingly, although surficial depth does not affect either deep-alluvium AAI or PTn AAI, and both colluvium porosity and colluvium depth scale colluvium/fracture AAI identically, multiplying the two input parameters by the same factor does not not yield the same relative change in AAI (2.2 versus 1.7). This apparent anomaly is due to the dual role of colluvium depth, which also is used to differentiate between the deep alluvium zone and the colluvium/fracture zone. Increasing surficial depth over the entire area increases the area classed as relatively low-AAI deep alluvium.

Several trends are obvious from the sensitivity coefficients presented in Table 6. In general, areal-average AAI is most sensitive to systematic variation in AAP and AAT. The input variables causing the next largest response are the colluvium/fracture system parameters, with porosity causing larger variation than I_D. The deep-alluvium hydraulic properties cause relatively small variation in areal-average AAI, as the areally integrated AAI within the deep alluvium zones is much smaller than the areally integrated AAI over regions with shallow colluvium. Similarly, variation in local AAI within PTn outcrop areas also has little impact on areal-average AAI due to the small outcrop area, especially within the 12 km^2 area centered on the repository footprint.

Raising the deep-alluvium k has relatively little impact on the areal-average AAI, decreasing it by about 0.5 mm/yr; however, the sensitivity coefficient of each deep-alluvium parameter decreases significantly while the sensitivity coefficients for the PTn and colluvium/fracture properties increase in magnitude slightly. Similar behavior would be expected if the alluvium k was less than 10^{-10} cm^2, as again the contribution of the deep alluvium to areal-average AAI becomes negligible. Thus, a zone can have a large relative change in the AAI within the zone due to a changing parameter, yet have a low sensitivity coefficient for the parameter, if the zone contributes a small amount of AAI to the total AAI over the entire region.

Enhancing colluvium/fracture AAI by halving all colluvium and alluvium depths increases areal-average AAI by a factor of 1.7, but decreases every sensitivity coefficient including the sensitivity coefficients for meteorological inputs. Enhancing colluvium/fracture AAI by modifying I_D or porosity also decreases every sensitivity coefficient, except that the sensitivity coefficients for meteorological inputs increase in magnitude. Enhancing AAI for every zone, either by increasing AAP or by decreasing AAT, has a mixed effect on sensitivity coefficients.

8 CONCLUSIONS

The spatial distribution of annual-average infiltration below the active evapotranspiration zone is of great interest for evaluating the performance of the proposed high-level waste repository at Yucca Mountain. In order to address the issue, numerical studies examining the sensitivity of AAI to various hydraulic and meteorologic parameters were undertaken. *Stothoff* [1996] examined the influence of hydraulic parameters on AAI, finding that for a 1D bare-soil system with colluvium overlying a fracture continuum, depth of colluvium is the dominant influence on AAI. The hydraulic properties of colluvium are also significant in estimating AAI. The underlying fractured-medium properties do not affect AAI significantly, as long as the fracture density is great enough to accept water pulses. Comparing the magnitude of variability in AAI that might occur due to the variability in hydraulic properties with the magnitude of variability in AAI that might occur solely due to the spatial distribution of meteorologic inputs, it might be concluded that capturing the hydraulic properties is more critical to predicting AAI at any particular location in space and the single most critical parameter to capture in 1D systems is the depth of cover over bedrock.

Functional relationships were developed to quantify the effect of hydraulic properties and annual-average meteorologic inputs on AAI for both deep alluvium and shallow colluvium/fracture systems. It was found that, in general, as AAI decreases the sensitivity of AAI to meteorologic influences increases.

With sensitivity information in hand, application to the Yucca Mountain site requires a plausible estimate of alluvial depth over the entire Yucca Mountain site. A simple erosion-balance model is proposed, which provides qualitatively correct alluvium depths. Combining the predicted alluvium depths with reasonable hydraulic parameters, predictions of AAI suggest that ridgetops, sideslopes, and headwaters of washes are primary locations for infiltration. The model also suggests that little or no infiltration will occur wherever alluvium is greater than a few tens of centimeters in depth.

The relative influences of hydraulic properties and meteorologic inputs on average AAI over the Yucca Mountain site were assessed. It was found that, of the meteorologic parameters, AAP and AAT have the greatest effect on AAI, but at the Yucca Mountain scale the spatial distribution of these factors is not large enough to have a great impact on AAI relative to variation in AAI due to potential variability in hydraulic properties. Interestingly, however, when AAP and AAT are changed simultaneously over the entire study site, perhaps due to climate change, the impact on areal-average AAI is much larger. With plausible ranges of parameter values, areal-average

AAI is more sensitive to systematic changes in AAP than to systematic changes in any hydraulic parameter. As might be expected, factors influencing large numbers of pixels (e.g., meteorologic inputs) or pixels with the largest contribution to the areal-average AAI (e.g., colluvium/fracture parameters) have the largest sensitivity coefficients. Factors that strongly affect a small number of pixels (e.g., AAI in PTn) or only affect pixels with a small relative AAI (e.g., deep-alluvium parameters) have low sensitivity coefficients.

Although the meteorological record is too short to provide truly representative long-term infiltration behavior for this semi-arid site, significant insight on expected infiltration behavior is gained. There are obvious limitations in the approach, as lateral redistribution, stratification, fast pathways, vegetation, matrix-fracture interactions, and fracture fillings are not considered. It is expected that neglecting vegetation, in particular, introduces a consistent bias towards overpredicting AAI, so that the predictions presented here are better considered upper-bound estimates. Nevertheless, based on the analysis, it can be concluded that in order to quantify the spatial distribution of infiltration at Yucca Mountain, it is particularly important to characterize flow processes occurring in areas with the shallowest colluvium depths over a fractured medium.

This paper was prepared to document work performed by the Center for Nuclear Waste Regulatory Analyses (CNWRA) for the NRC under Contract No. NRC-02-93-005. The activities reported here were performed on behalf of the NRC Office of Nuclear Material Safety and Safeguards, Division of Waste Management, and the NRC Office of Nuclear Regulatory Research, Division of Regulatory Applications. The paper is an independent product of the CNWRA and does not necessarily reflect the views or regulatory position of the NRC. The BREATH code used in this paper is configured under the CNWRA's Software Configuration Procedure. The authors would like to acknowledge the suggestions and comments made by Ronald Green, Gordon Wittmeyer, and Patrick Mackin, which tremendously improved the quality of the paper.

9 REFERENCES

Ackers, P. and W. R. White. 1973. Sediment Transport: New Approach and Analysis. *Journal of the Hydraulics Division, American Society of Civil Engineers 99*(HY11), 2041–2060.

Beaumont, C., P. Fullsack, and J. Hamilton. 1992. Erosional control of active compressional orogens. In K. R. McClay (Ed.), *Thrust Tectonics*, London, pp. 1–18. Chapman & Hall.

Fair, G. M. and J. C. Geyer. 1954. *Water Supply and Wastewater Disposal.* New York, NY: John Wiley & Sons.

Fairbridge, R. W. (Ed.). 1967. *The Encyclopedia of Atmospheric Sciences and Astrogeology.* New York, NY: Reinhold Publishing Corporation.

Fernandez, J. A., J. B. Case, C. A. Givens, and B. C. Carney. 1994. *A Strategy to Seal Exploratory Boreholes in Unsaturated Tuff.* SAND93-1184, Sandia National Laboratories, Albuquerque, NM.

Flint, A. L. and L. E. Flint. 1994. Spatial Distribution of Potential Near Surface Moisture Flux at Yucca Mountain. In *Proceedings of the Fifth Annual High Level Radioactive Waste Management Conference*, La Grange Park, IL, pp. 2352–2358. American Nuclear Society.

Flint, A. L., L. E. Flint, and J. A. Hevesi. 1993. The Influence of Long Term Climate Change on Net Infiltration at Yucca Mountain. In *Proceedings of the Fourth Annual High Level Radioactive Waste Management Conference*, La Grange Park, IL, pp. 152–159. American Nuclear Society.

Flint, L. E., A. L. Flint, and J. A. Hevesi. 1994. Shallow Infiltration Processes in Arid Watersheds at Yucca Mountain, Nevada. In *Proceedings of the Fifth Annual High Level Radioactive Waste Management Conference*, La Grange Park, IL, pp. 2315–2322. American Nuclear Society.

Flint, L. E., A. L. Flint, T. Moyer, and J. Geslin. 1995. Lateral Diversion of Water in the Paintbrush Tuff Nonwelded Hydrologic Unit, Yucca Mountain, Nevada. In *Supplement to Eos, Transactions*, Volume 76, Washington, DC, pp. F182. American Geophysical Union.

Freeze, R. A. and J. A. Cherry. 1979. *Groundwater.* Englewood Cliffs, NJ: Prentice-Hall, Inc.

Hevesi, J. A. and A. L. Flint. 1993. The Influence of Seasonal Climatic Variability on Shallow Infiltration at Yucca Mountain. In *Proceedings of the Fourth Annual High Level Radioactive Waste Management Conference*, La Grange Park, IL, pp. 122–131. American Nuclear Society.

Hevesi, J. A., A. L. Flint, and L. E. Flint. 1994. Verification of a 1-Dimensional Model for Predicting Shallow Infiltration at Yucca Mountain. In *Proceedings of the Fifth Annual High Level Radioactive Waste Management Conference*, La Grange Park, IL, pp. 2323–2332. American Nuclear Society.

Hevesi, J. A., J. D. Istok, and A. L. Flint. 1992. Precipitation Estimation in Mountainous Terrain Using Multivariate Geostatistics. Part I: Structural Analysis. *Journal of Applied Meteorology 31*(7), 661–676.

Hudson, D. B., A. L. Flint, and W. R. Guertal. 1994. Modeling a Ponded Infiltration Experiment at Yucca Mountain, NV. In *Proceedings of the Fifth Annual High Level Radioactive Waste Management Conference*, La Grange Park, IL, pp. 2168–2174. American Nuclear Society.

Kilinc, M. and E. V. Richardson. 1973. *Mechanics of Soil Erosion From Overland Flow Generated by Simulated Rainfall.* Hydrology Paper 63, Colorado State University, Fort Collins, CO.

Kwicklis, E. M., A. L. Flint, and R. W. Healy. 1994. Simulation of Flow in the Unsaturated Zone Beneath Pagany Wash, Yucca Mountain. In *Proceedings of the Fifth Annual High Level Radioactive Waste Management Conference*, La Grange Park, IL, pp. 2341–2351. American Nuclear Society.

Long, A. and S. W. Childs. 1993. Rainfall and Net Infiltration Probabilities for Future Climate Conditions at Yucca Mountain. In *Proceedings of the Fourth Annual High Level Radioactive Waste Management Conference*, La Grange Park, IL, pp. 112–121. American Nuclear Society.

McKinley, P. and T. Oliver. 1994. *Meteorological, Stream-Discharge, and Water-Quality Data for 1986 through 1991 from Two Small Basins in Central Nevada.* Open-File Report 93-651, United States Geological Survey, Denver, CO.

Meyer, L. D. and W. H. Wischmeier. 1969. Mathematical Simulation of the Process of Soil Erosion by Water. *Transactions of the American Society of Agricultural Engineers 12*(6), 754–762.

National Climatic Data Center. 1984 to 1994. *WBAN Hourly Surface Observations.* Asheville, NC: National Oceanic and Atmospheric Administration.

Nuclear Regulatory Commission. 1992. *Initial Demonstration of the NRC's Capability to Conduct a Performance Assessment for a High-Level Waste Repository.* NUREG-1327, Nuclear Regulatory Commission, Washington, DC.

Nuclear Regulatory Commission. 1995. *NRC Iterative Performance Assessment Phase 2: Development of Capabilities for Review of a Performance Assessment for a High-Level Waste Repository.* NUREG-1464, Nuclear Regulatory Commission, Washington, DC.

Sandia National Laboratories. 1992. *TSPA 1991: An Initial Total-System Performance Assessment for Yucca Mountain.* SAND91-2795, Sandia National Laboratories, Albuquerque, NM.

Sandia National Laboratories. 1994. *Total-System Performance Assessment for Yucca Mountain–SNL Second Iteration (TSPA-1993).* SAND93-2675, Sandia National Laboratories, Albuquerque, NM.

Schenker, A. R., D. C. Guerin, T. H. Robey, C. A. Rautman, and R. W. Barnard. 1995. *Stochastic Hydrogeologic Units and Hydrogeologic Properties Development for Total-System Performance Assessments.* SAND94-0244, Sandia National Laboratories, Albuquerque, NM.

Scott, R. B. and J. Bonk. 1984. *Preliminary Geologic Map (1:12,000 scale) of Yucca Mountain, Nye County, Nevada, with Geologic Cross Sections.* Open-File Report 84-494, United States Geological Survey, Denver, CO.

Stirewalt, G. L. and D. B. Henderson. 1995. A Preliminary Three-Dimensional Geological Framework Model for Yucca Mountain. In *Proceedings of the Sixth Annual High Level Radioactive Waste Management Conference*, La Grange Park, IL, pp. 116–118. American Nuclear Society.

Stothoff, S. A. 1995. *BREATH Version 1.1–Coupled Flow and Energy Transport in Porous Media: Simulator Description and User Guide.* NUREG/CR 6333, Nuclear Regulatory Commission, Washington, DC.

Stothoff, S. A. 1996. Sensitivity of Long-Term Bare-Soil Infiltration Simulations to Hydraulic Properties in an Arid Environment. *Water Resources Research.* Submitted.

Sykes, J. F., J. L. Wilson, and R. W. Andrews. 1985. Sensitivity Analysis for Steady State Groundwater Flow Using Adjoint Operators. *Water Resources Research 21*(3), 359–371.

TRW. 1995. *Total System Performance Assessment–1995: An Evaluation of the Potential Yucca Mountain Repository.* B00000000-01717-2200-00136, TRW Environmental Safety Systems Inc., Las Vegas, NV.

Woolhiser, D. A., R. E. Smith, and D. C. Goodrich. 1990. *KINEROS, A Kinematic Runoff and Erosion Model: Documentation and User Manual.* ARS-77, United States Department of Agriculture, Agricultural Research Service.

Yalin, Y. S. 1963. An Expression for Bed-Load Transportation. *Journal of the Hydraulics Division, American Society of Civil Engineers 89*(HY3), 221–250.

Yang, C. T. 1973. Incipient Motion and Sediment Transport. *Journal of the Hydraulics Division, American Society of Civil Engineers 99*(HY10), 1679–1704.

Table 1: Regressed coefficients for deep-alluvium AAI response to meteorologic inputs.

Coefficient	$k = 10^{-8}$ cm^2	$k = 10^{-5}$ cm^2
β_0	-4.7	-4.9
β_1	1.2	1.8
β_2	1.8	3.3
β_3	8.9	25
β_4	0.19	0.41
β_5	0.12	0.53

Table 2: Regressed coefficients for colluvium/fracture AAI response to meteorologic inputs.

Coefficient	Value	Coefficient	Value
j_0	-7.72×10^{-4}	j_1	0.679
j_2	-5.30	j_3	-0.739
j_4	16.2	j_5	60.9
j_6	0.868	j_7	-18.8
j_8	-142	j_9	-1240

Table 3: Maximum AAI divided by minimum AAI over the Yucca Mountain DEM, varying each meteorologic input parameter one at a time or varying all meteorologic input parameters simultaneously.

	Varied Meteorologic Input Parameter				
Permeability	AAP	AAT	AAV	Solar	All
10^{-8} cm^2	2.9	1.7	1.09	1.3	4.9
10^{-5} cm^2	3.2	5.1	1.33	1.6	14.2

Table 4: Adjustable parameters for creating colluvium distributions.

Name	Symbol	Base Value
Net rainfall rate	q_{rain}	5 cm/hr
Manning's roughness coefficient	n	0.1
Kinetic coefficient for alluvium scour	C_g	0.1 s^{-1}
Kinetic coefficient for bedrock scour	C_g	0.002 s^{-1}
Traction coefficient for sediment equilibrium	C_s	10^{-3}
Particle diameter	d	1 mm
Particle specific gravity	S_s	2.5
Alluvium creep conductance	K	10^{-12} m/s
Alluvium weathering rate	Q_0	10^{-9} m^3/m^2s
Alluvium weathering depth	b_0	1 cm
Fraction of time in streamflow	F_{str}	30 min/100 yr

Table 5: Parameter values used for sensitivity coefficient estimation.

Parameter	Base Case			Alternate Base Value			
	Low	Reference	High	Low	Reference	High	Rel. *AAI*
Alluvium k (cm^2)	10^{-6}	10^{-7}	10^{-8}	10^{-5}	10^{-6}	10^{-7}	0.966
Alluvium m	0.1	0.2	0.3	–	–	–	–
Alluvium P_0 ($\times 10^3$ Pa)	1	2	5	–	–	–	–
Alluvium porosity ε_a	0.1	0.2	0.5	–	–	–	–
AAP fraction in PTn	0.0	0.1	0.2	–	–	–	–
I_{D0}	0.5	0.7	0.9	0.4	0.6	0.8	1.13
Colluvium porosity ε_c	0.1	0.2	0.3	0.05	0.1	0.15	2.2
Depth multiplier	0.5	1	2	0.25	0.5	1	1.7
AAP multiplier	0.67	1	1.5	1	1.5	2.25	3.1
AAT shift (°C)	−3	+3	+3	−6	+3	0	2.0

Table 6: Relative change in AAI used to calculate base-case sensitivity coefficients and the AAI sensitivity coefficient values for the base case and cases resulting from systematically changing parameters.

	Relative AAI		Sensitivity Coefficient						
	Perturbation		Base	Alternate Base Value					
Parameter	Low	High	Case	k	I_{D0}	ε_c	Depth	AAP	AAT
k	1.11	0.965	-0.014	-0.005	-0.013	-0.007	-0.008	-0.014	-0.008
m	0.967	1.24	+0.271	+0.089	+0.239	+0.126	+0.156	+0.339	+0.186
P_0	1.20	0.961	-0.121	-0.040	-0.106	-0.056	-0.070	-0.152	-0.083
ε_a	1.05	0.975	-0.077	-0.025	-0.067	-0.035	-0.044	-0.096	-0.053
PTn	0.966	1.03	+0.034	+0.035	+0.030	+0.016	+0.019	+0.011	+0.017
I_{D0}	1.27	0.749	-0.914	-0.947	-0.683	-0.348	-0.261	-1.12	-1.19
ε_c	2.16	0.556	-1.60	-1.66	-1.40	-1.06	-0.99	-1.63	-1.39
Depth	1.73	0.463	-0.848	-0.878	-0.700	-0.441	-0.585	-0.499	-0.470
AAP	0.289	3.05	+3.33	+3.31	+3.43	+3.38	+2.47	+2.63	+2.44
AAT	2.04	0.609	-0.715	-0.731	-0.760	-0.814	-0.441	-0.442	-1.14

Figure 1: Long-term net infiltration for two semi-infinite alluvium columns with different k, and with uniformly perturbed meteorological parameters.

Figure 2: Long-term net infiltration in two semi-infinite columns as a function of long-term average deep saturation: (a) unscaled, (b) scaled AAI and normalized AAS.

Figure 3: Response of simulation AAI to AAT and AAP for shallow colluvium overlying a fracture continuum.

Figure 4: Simulated and approximated AAI for permeability and: (a) van Genuchten m (labeled m), (b) bubbling pressure (10^3 Pa) (labeled P0), and (c) porosity (labeled poros).

Figure 5: The response of normalized AAI to depth of colluvium, with different values of porosity, for base-case meteorology and shallow colluvium overlying a fracture continuum.

Figure 6: Normalized AAI compared to the approximation for normalized AAI.

Figure 7: The ratio of AAI to base-case AAI due to variation of meteorological factors, assuming uniform coverage of semi-infinite base-case alluvium.

Figure 8: Hydraulic depth distribution calculated by the water-balance model, with $q_{rain} = 5$ cm/hr and $n = 0.1$.

Figure 9: Sediment concentration distribution calculated by the sediment-balance model, with $q_{rain} = 5$ cm/hr.

Figure 10: Colluvium depth distribution calculated by the erosion-balance model, with $Q_0 = 10^{-7}$ s^{-1}, $b_0 = 1$ cm, $q_{rain} = 5$ cm/hr, and $K = 10^{-10}$ m^2/s.

Figure 11: Base-case colluvium depth distribution with regressed alluvium depths within the mapped alluvium outline.

Figure 12: Unit classification for the estimation of the spatial distribution of infiltration, based on the CNWRA 3D GFM.

Figure 13: Example spatial distribution of AAI, accounting for depth of alluvium, underlying bedrock, and meteorological effects.

Figure 14: Scatterplot of calculated AAI versus alluvium depth for the case presented in Figure 13.

FIGURE 1

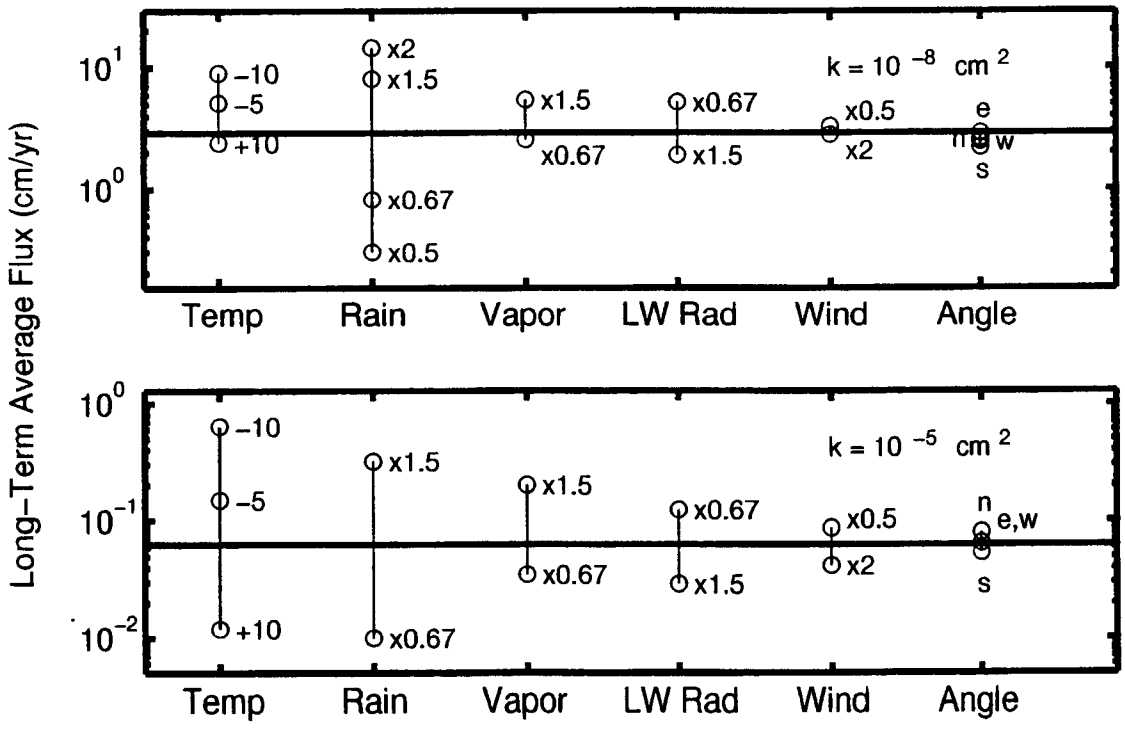
Long-Term Average Flux (cm/yr)
10^1
10^0
10^{-1}
10^{-2}
k = 10^{-8} cm^2
k = 10^{-5} cm^2
−10
−5
+10
x2
x1.5
x0.67
x0.5
x1.5
x0.67
x0.67
x1.5
x0.5
x2
e
n
w
s
e,w
Temp
Rain
Vapor
LW Rad
Wind
Angle

FIGURE 2A

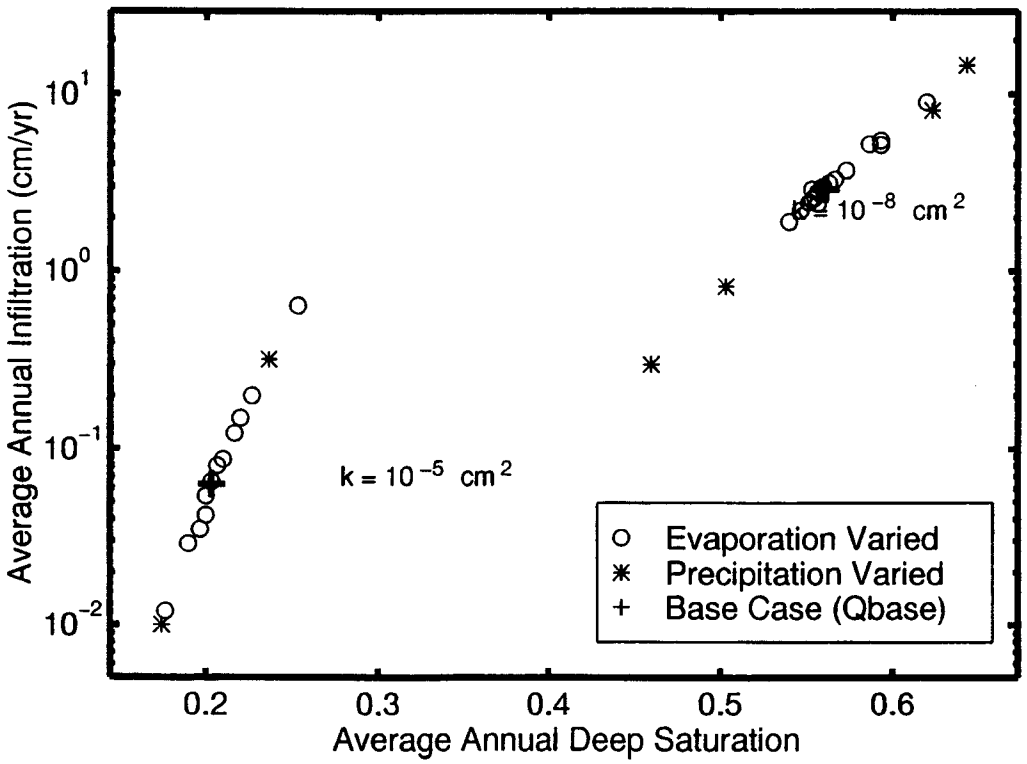
Average Annual Infiltration (cm/yr)
10^{1}
10^{0}
10^{-1}
10^{-2}
0.2
0.3
0.4
0.5
0.6
Average Annual Deep Saturation
$k = 10^{-8}$ cm^2
$k = 10^{-5}$ cm^2
Evaporation Varied
Precipitation Varied
Base Case (Qbase)

FIGURE 2B

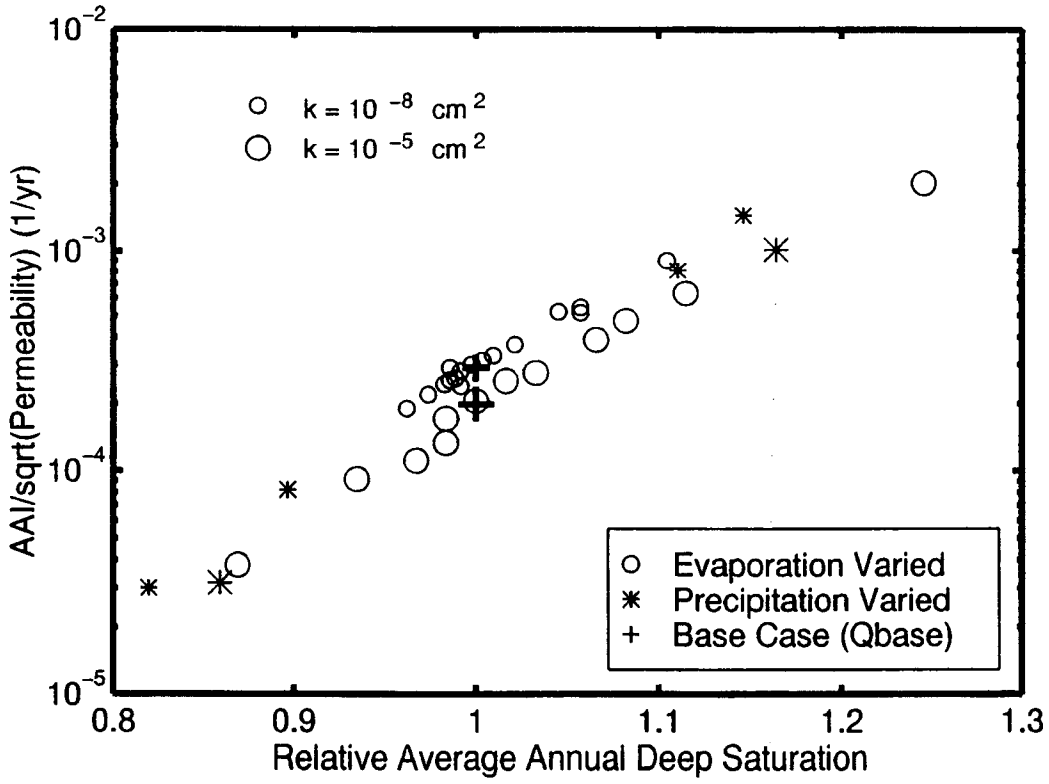
10^{-2}
10^{-3}
10^{-4}
10^{-5}
AAI/sqrt(Permeability) (1/yr)
k = 10^{-8} cm^2
k = 10^{-5} cm^2
Evaporation Varied
Precipitation Varied
Base Case (Qbase)
0.8
0.9
1
1.1
1.2
1.3
Relative Average Annual Deep Saturation

FIGURE 3

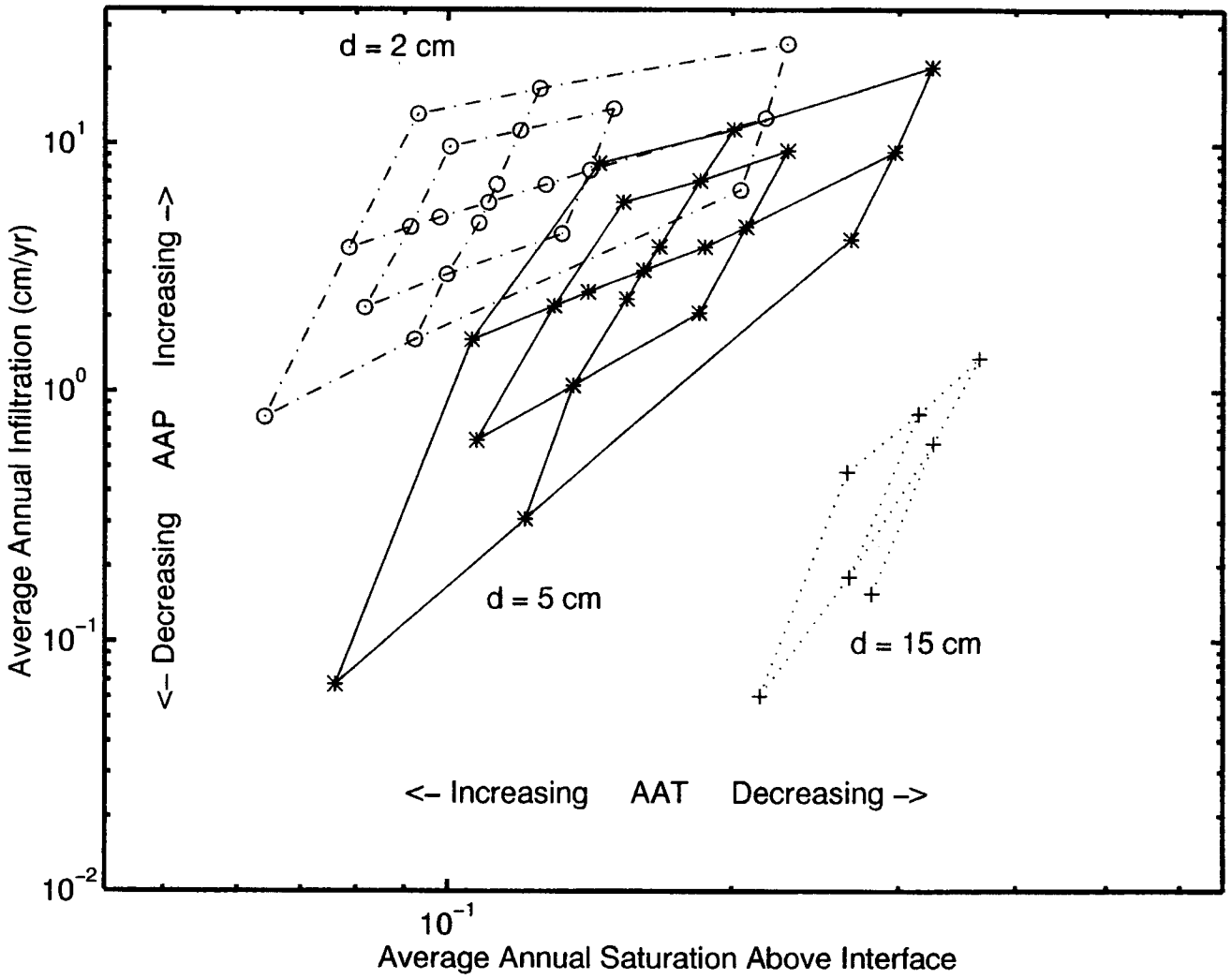
d = 2 cm
d = 5 cm
d = 15 cm
Average Annual Infiltration (cm/yr)
<– Decreasing AAP Increasing –>
<– Increasing AAT Decreasing –>
Average Annual Saturation Above Interface
10^{1}
10^{0}
10^{-1}
10^{-2}
10^{-1}

FIGURE 4A

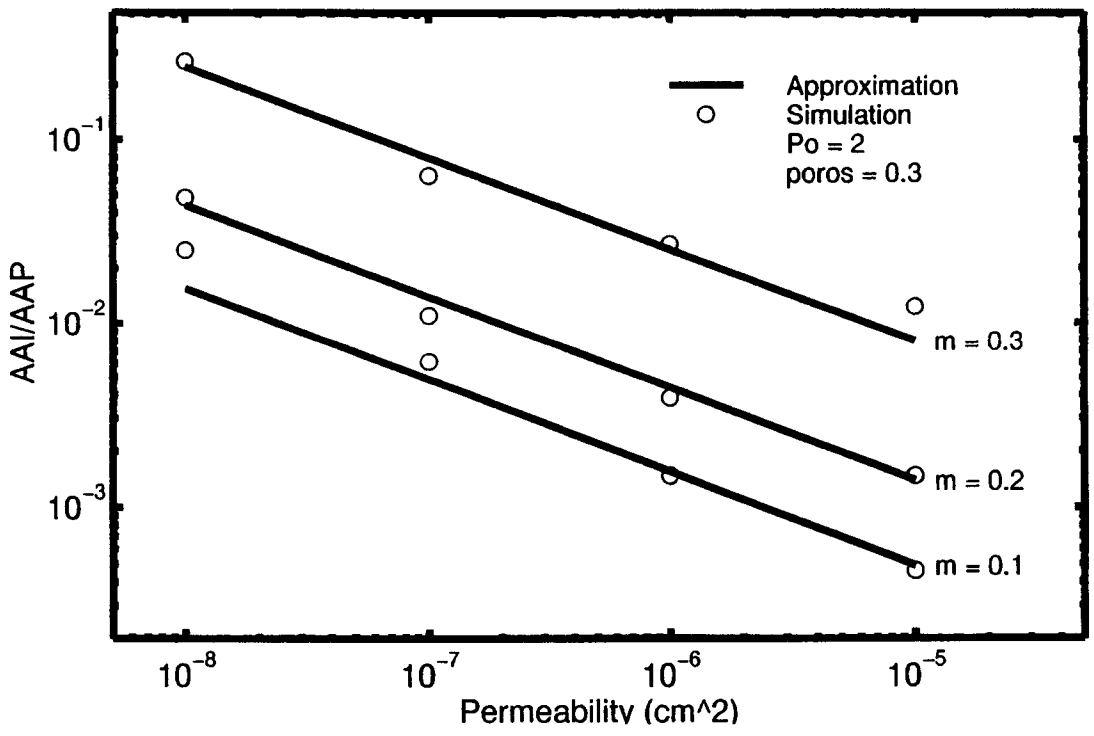
Approximation
Simulation
Po = 2
poros = 0.3
m = 0.3
m = 0.2
m = 0.1
AAI/AAP
10^{-1}
10^{-2}
10^{-3}
10^{-8}
10^{-7}
10^{-6}
10^{-5}
Permeability (cm^2)

FIGURE 4B

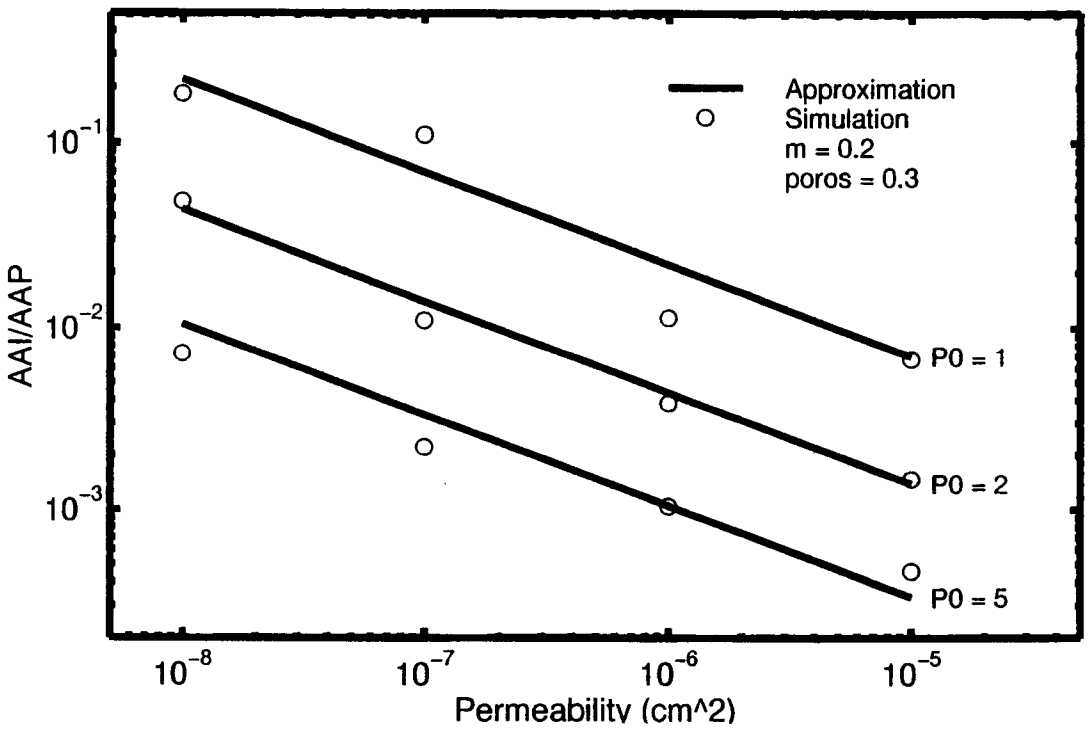
Approximation
Simulation
m = 0.2
poros = 0.3
P0 = 1
P0 = 2
P0 = 5
AAI/AAP
10^{-1}
10^{-2}
10^{-3}
10^{-8}
10^{-7}
10^{-6}
10^{-5}
Permeability (cm^2)

FIGURE 4C

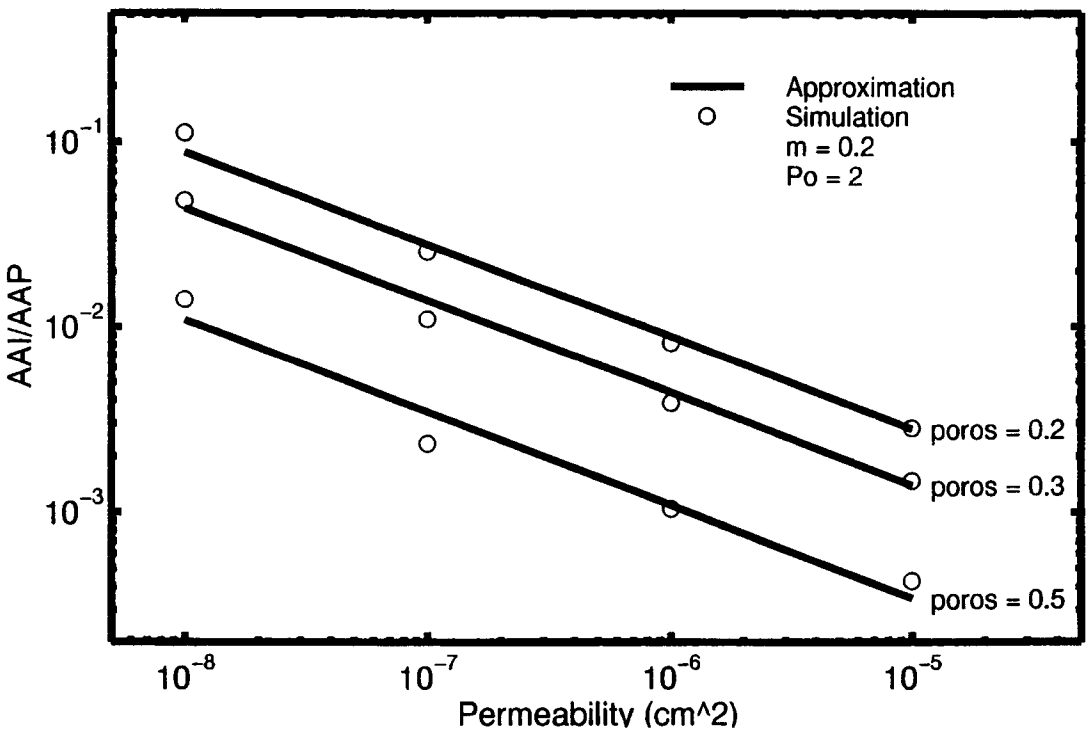
Approximation
Simulation
m = 0.2
Po = 2
AAI/AAP
10^{-1}
10^{-2}
10^{-3}
poros = 0.2
poros = 0.3
poros = 0.5
10^{-8}
10^{-7}
10^{-6}
10^{-5}
Permeability (cm^2)

FIGURE 5

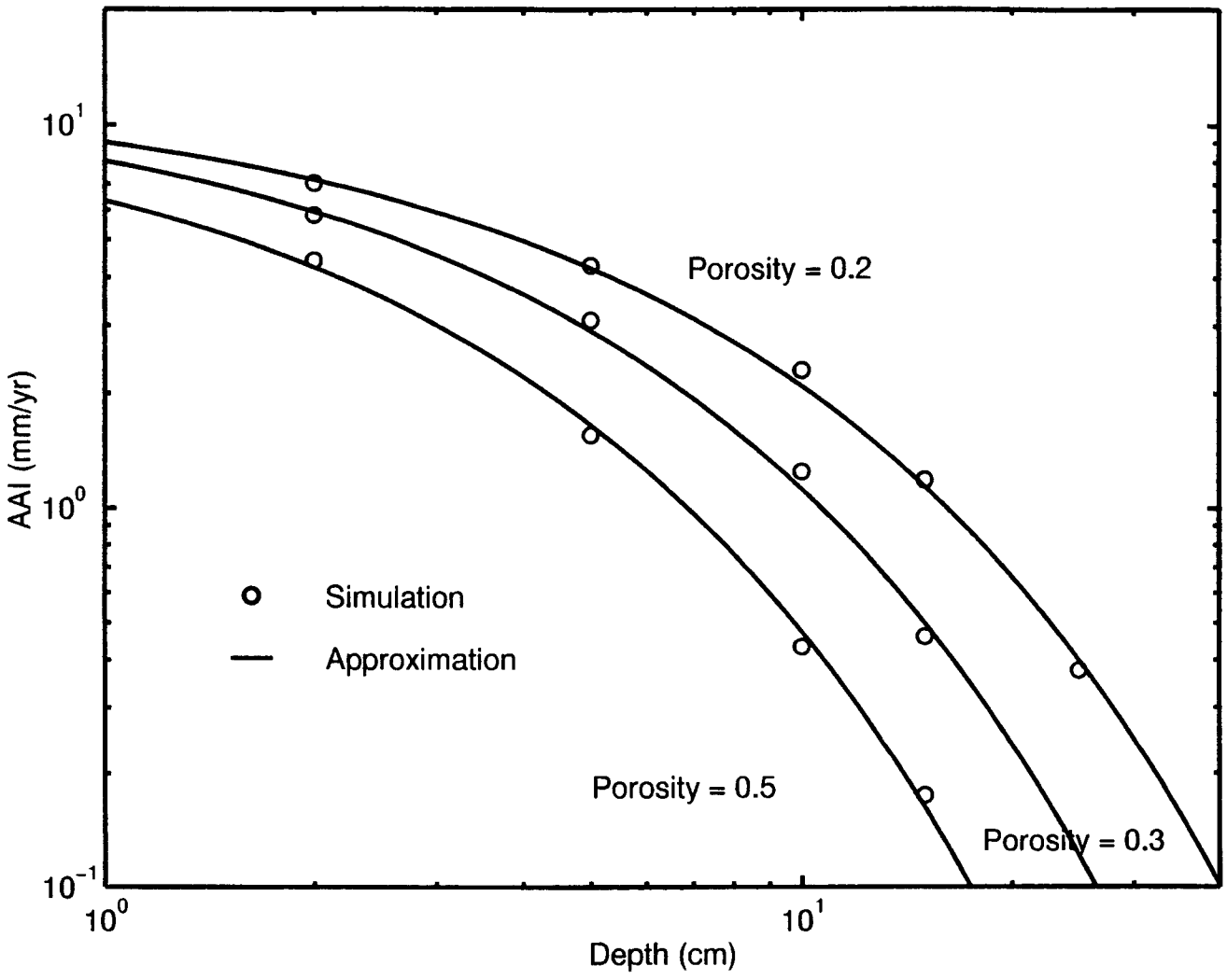
AAI (mm/yr)
10^1
10^0
10^{-1}
10^0
10^1
Depth (cm)
Simulation
Approximation
Porosity = 0.2
Porosity = 0.3
Porosity = 0.5

FIGURE 6

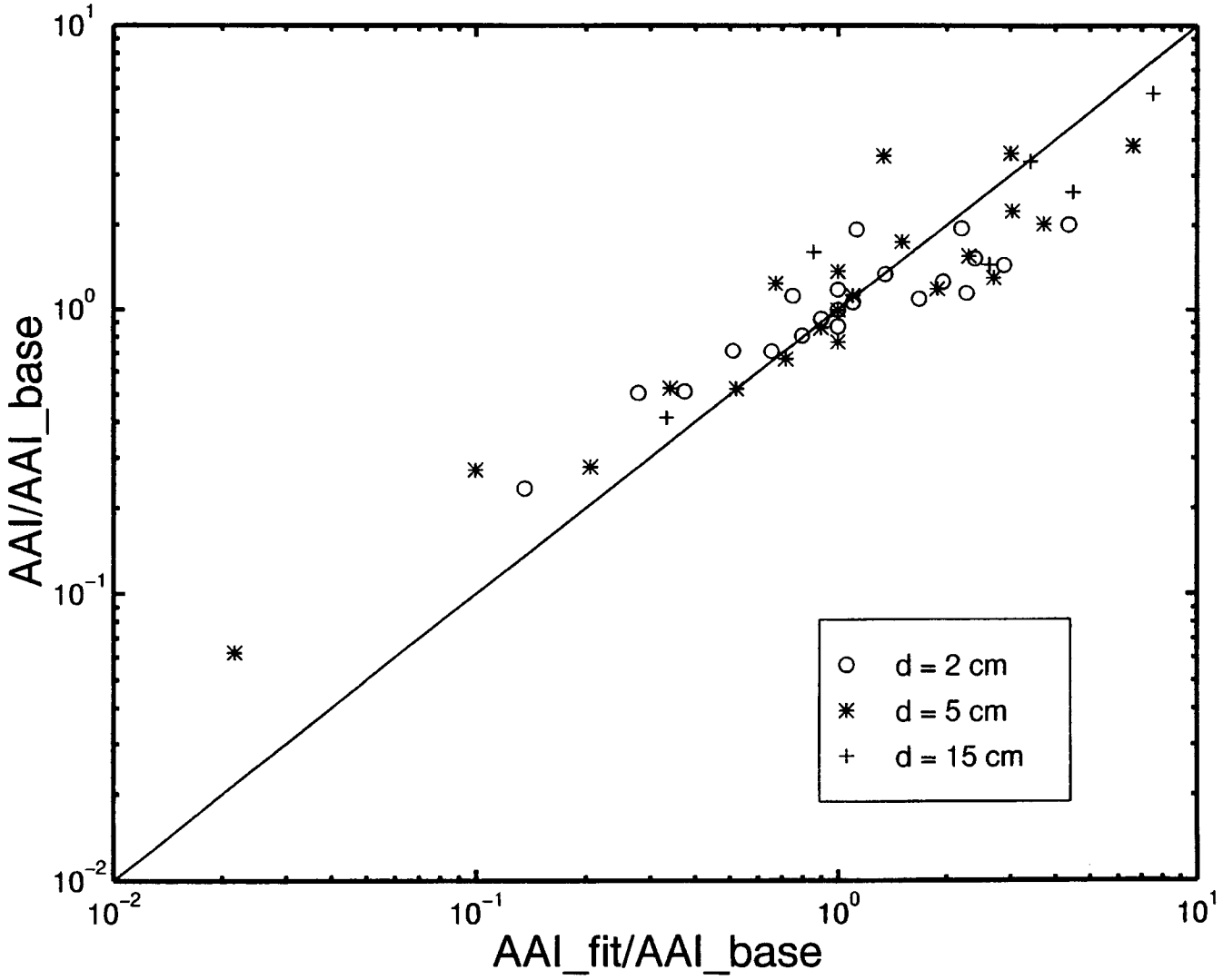
AAI/AAI_base
AAI_fit/AAI_base
10^{1}
10^{0}
10^{-1}
10^{-2}
10^{-2}
10^{-1}
10^{0}
10^{1}
d = 2 cm
d = 5 cm
d = 15 cm

FIGURE 7

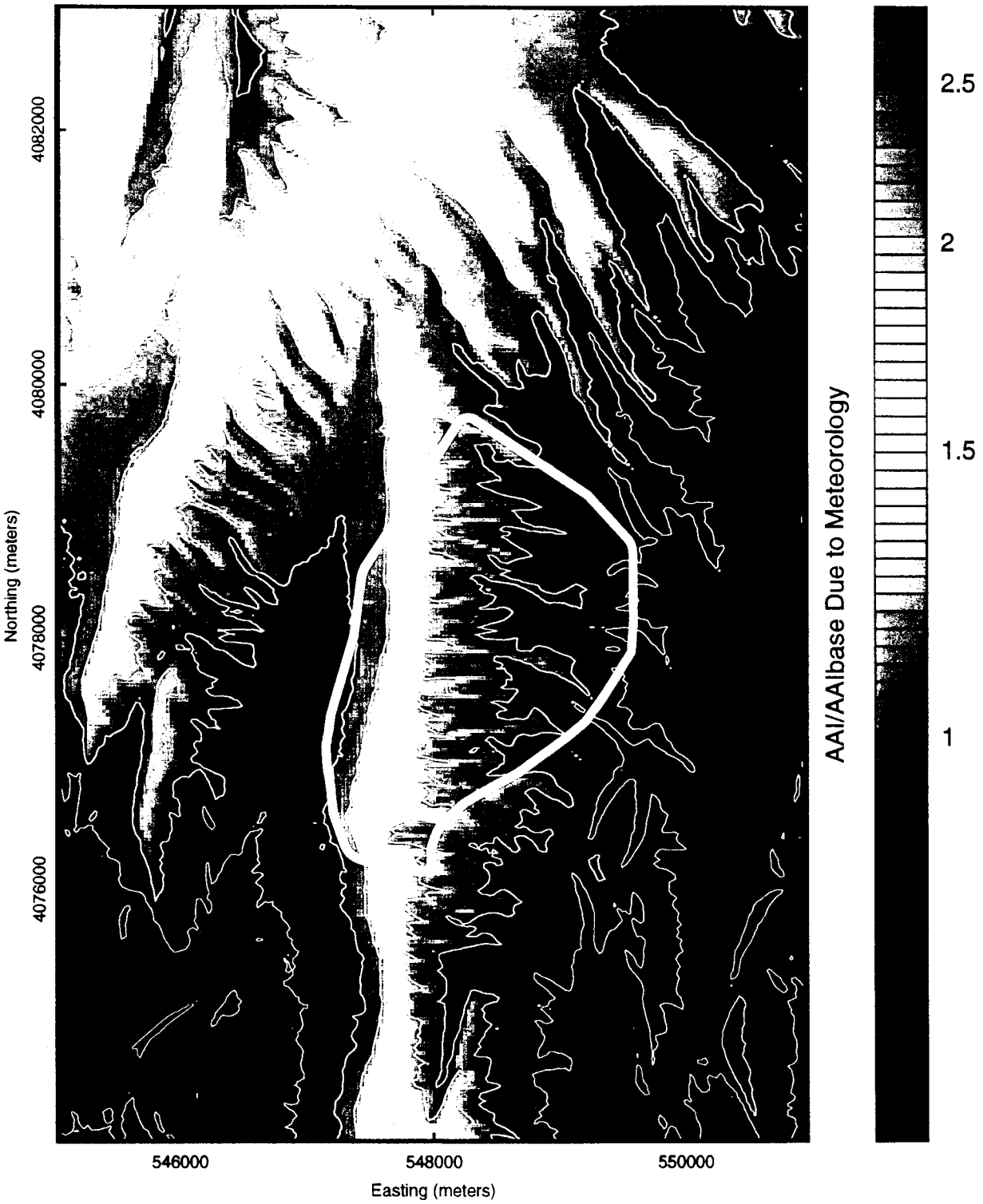
Northing (meters)
4082000
4080000
4078000
4076000
546000
548000
550000
Easting (meters)
AAI/AAIbase Due to Meteorology
2.5
2
1.5
1

FIGURE 8

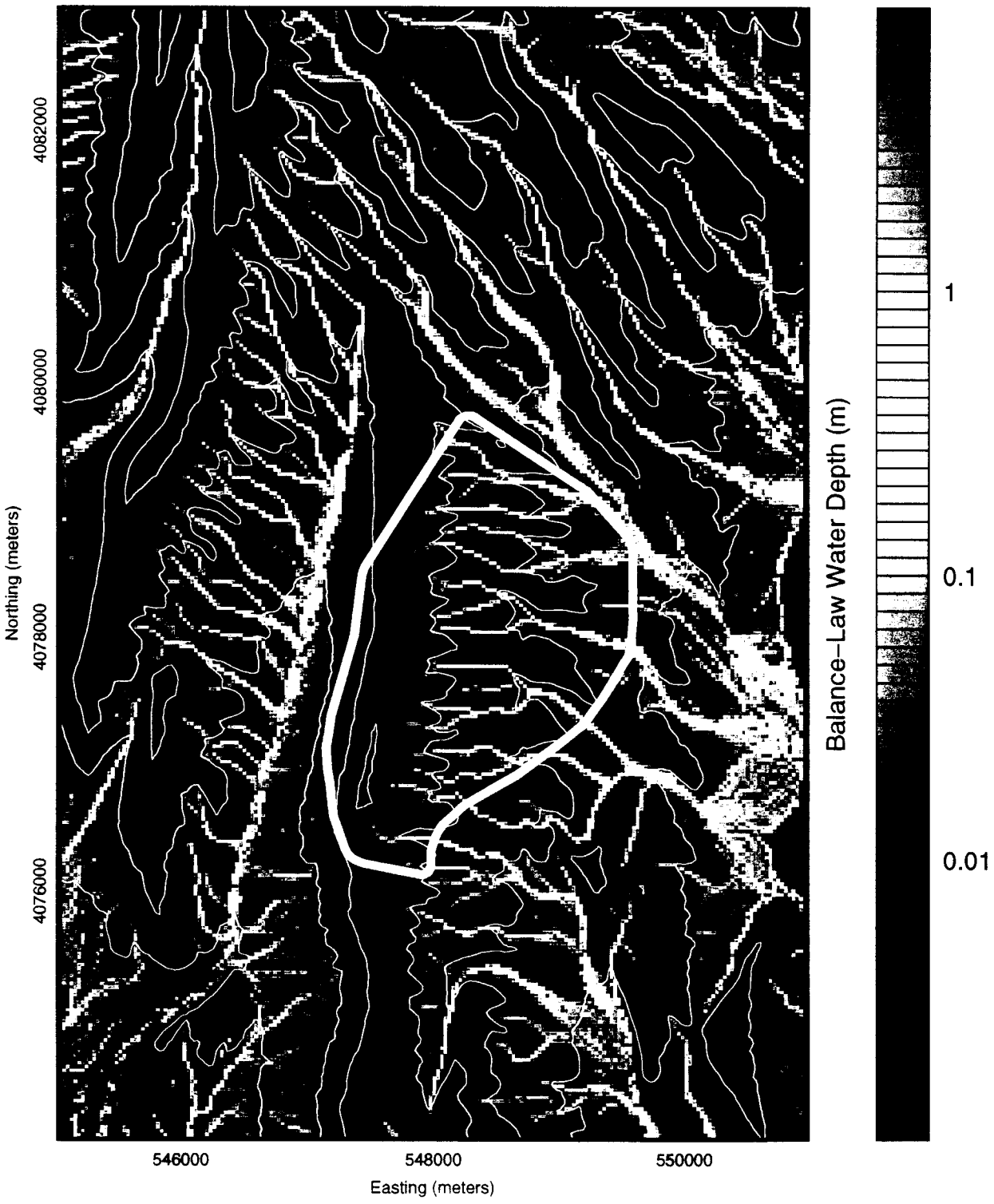
4082000
4080000
4078000
4076000
Northing (meters)
546000
548000
550000
Easting (meters)
Balance-Law Water Depth (m)
1
0.1
0.01

FIGURE 9

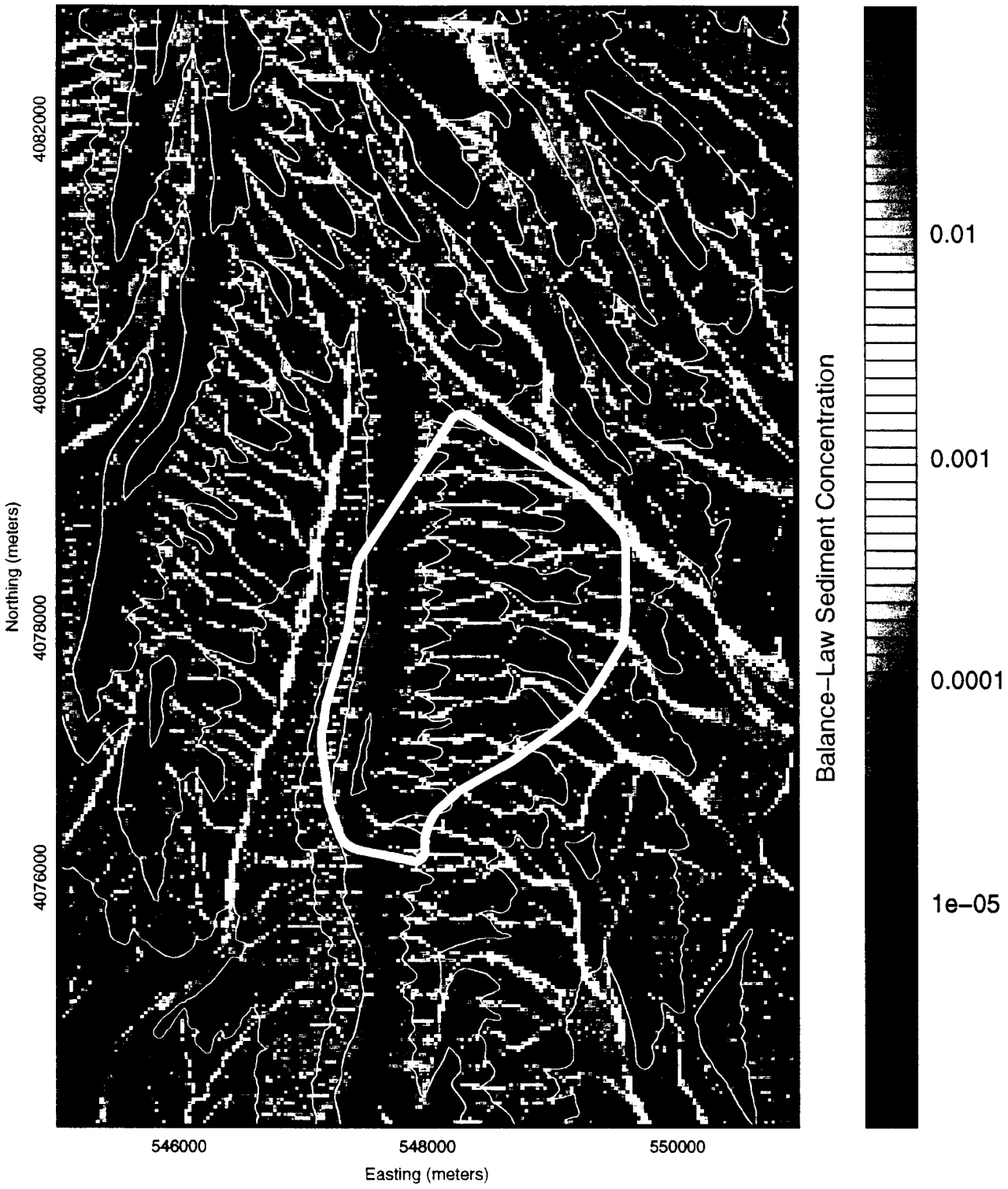
4082000
4080000
4078000
4076000
Northing (meters)
546000
548000
550000
Easting (meters)
Balance-Law Sediment Concentration
0.01
0.001
0.0001
1e-05

Figure 10


4082000
4080000
4078000
4076000
Northing (meters)
546000
548000
550000
Easting (meters)
Balance-Law Alluvium Depth (m)
10
1
0.1

Figure 11

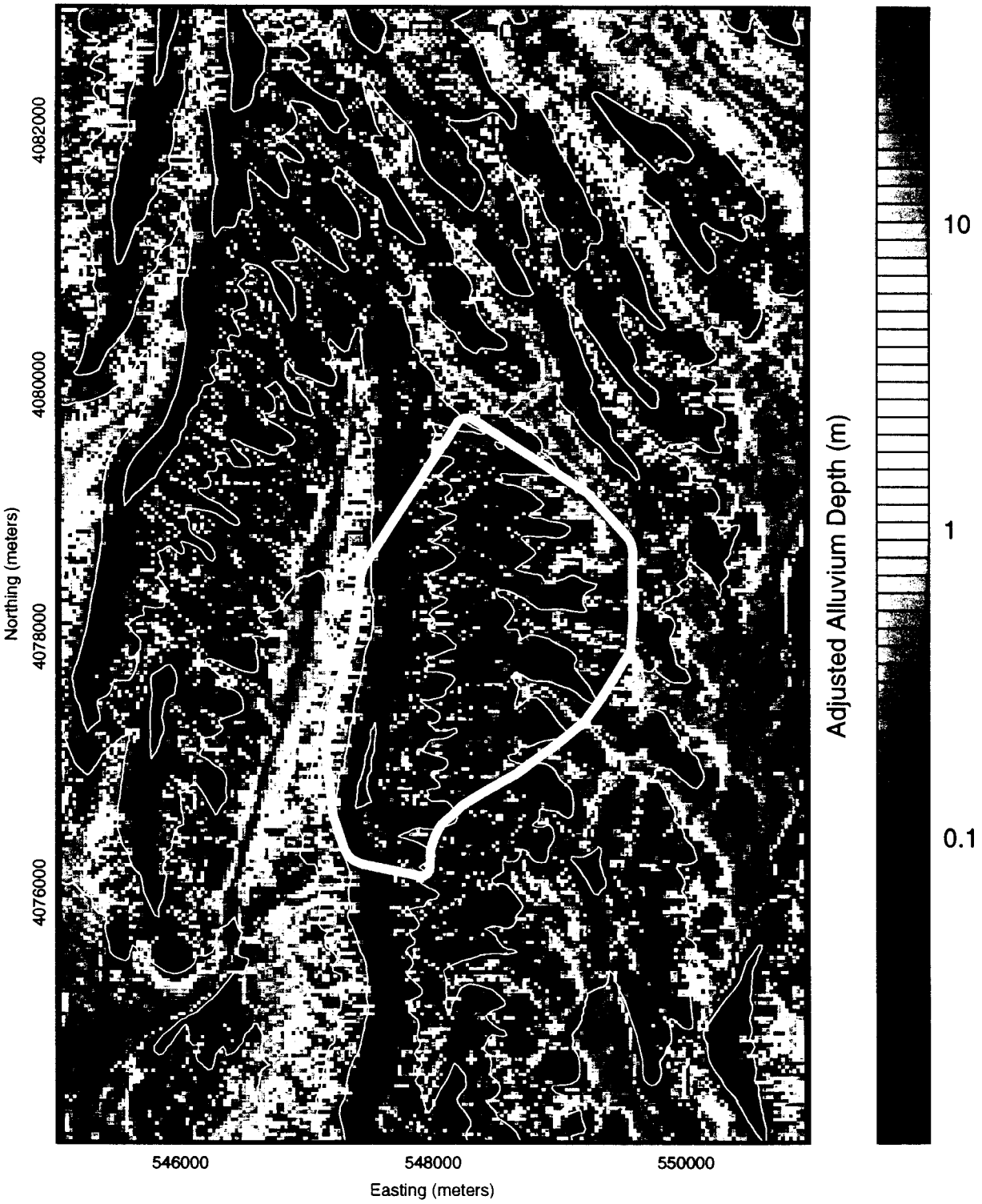
Northing (meters)
4082000
4080000
4078000
4076000
546000
548000
550000
Easting (meters)
Adjusted Alluvium Depth (m)
10
1
0.1

FIGURE 12

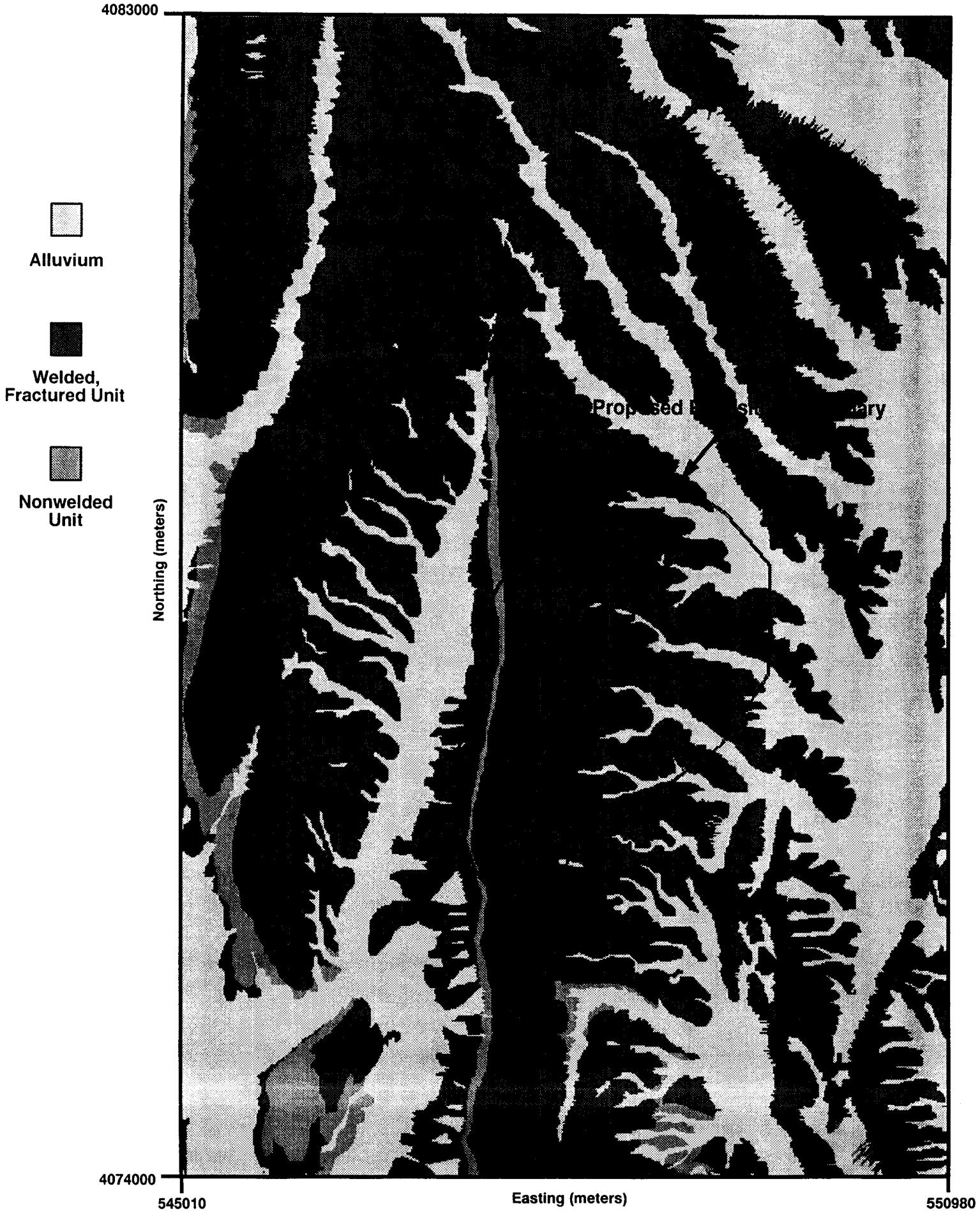
4083000
Alluvium
Welded, Fractured Unit
Nonwelded Unit
Northing (meters)
4074000
545010
Easting (meters)
550980

Figure 13

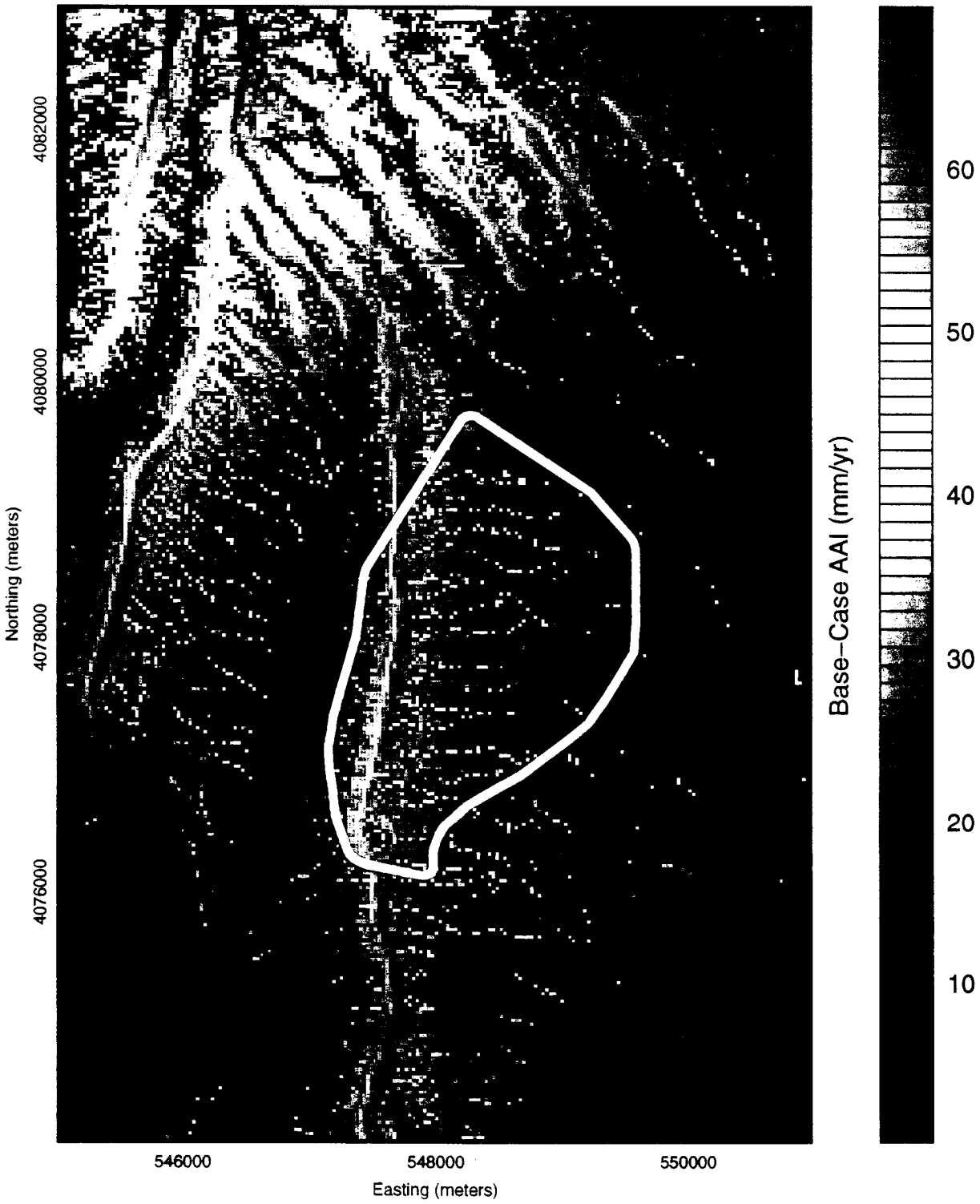
4082000
4080000
4078000
4076000
Northing (meters)
546000
548000
550000
Easting (meters)
Base-Case AAI (mm/yr)
60
50
40
30
20
10

FIGURE 14

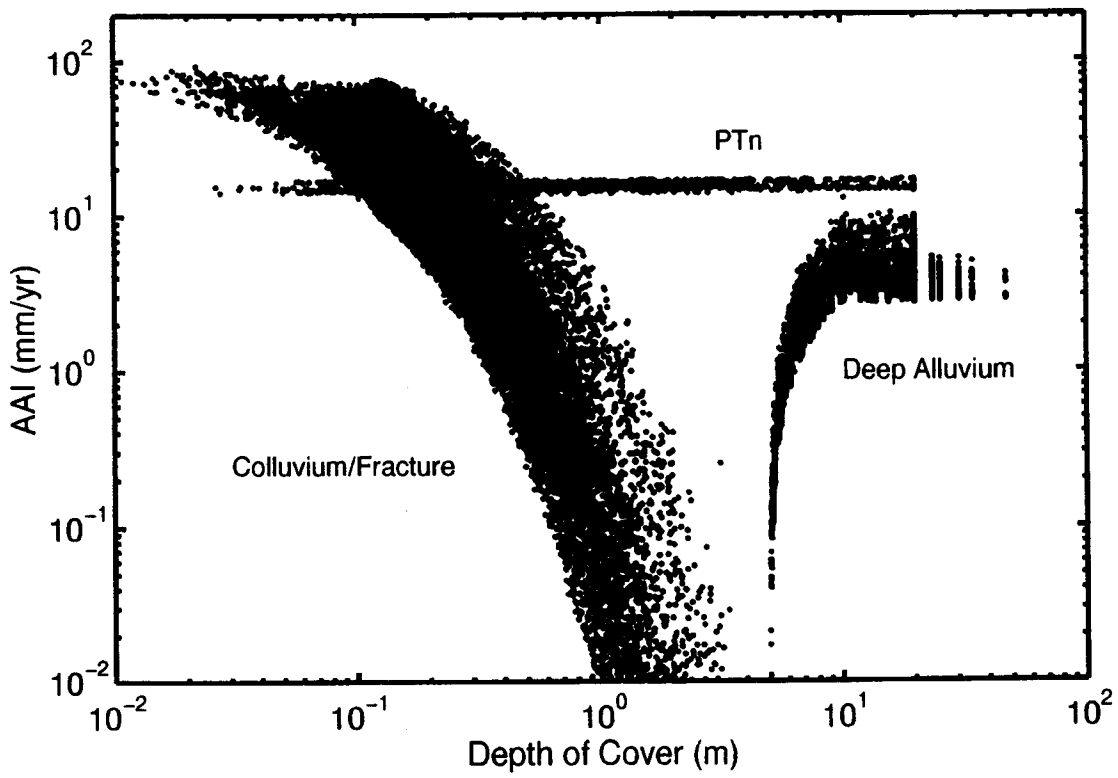
AAI (mm/yr)
10^2
10^1
10^0
10^{-1}
10^{-2}
PTn
Deep Alluvium
Colluvium/Fracture
10^{-2}
10^{-1}
10^0
10^1
10^2
Depth of Cover (m)